Catalysis Science & Technology

ROYAL SOCIETY OF CHEMISTRY

REVIEW

View Article Online
View Journal | View Issue

Cite this: *Catal. Sci. Technol.*, 2025, **15**, 5552

From CO_2 to DME: catalytic advances, challenges, and alternatives to conventional gas-phase routes

Elka Kraleva,*[a] Udo Armbruster,[a] Maria Luisa Saladino,[b] Francesco Giacalone,*[b] Tomoo Mizugaki[c] and Izabela S. Pieta*[d]

Received 14th April 2025,
Accepted 11th August 2025

DOI: 10.1039/d5cy00462d

rsc.li/catalysis

Dimethyl ether (DME) is gaining attention as both a biofuel and electro-fuel (e-fuel) due to its high volumetric energy density (0.16 kg H_2 per l) and rich hydrogen content, making it a promising energy carrier. Global DME production is around 10 million tons annually, primarily derived from synthesis gas. This process typically requires high temperatures above 250 °C and elevated pressures, involving two catalysts and multiple stages of separation and distillation. A major breakthrough in DME production would involve utilizing CO_2 and H_2 mixtures under milder conditions in a single-step process. Such advancements could create a circular DME synthesis–consumption cycle, leading to significant reductions in greenhouse gas (GHG) emissions. This work explores recent developments in both direct and indirect DME production methods, with a focus on enhancing CO_2-to-DME processes. It highlights the design of highly active, durable, and selective catalysts, as well as scalable synthesis methods that eliminate expensive separation and distillation steps. In addition to conventional gas-phase approaches, this review presents a novel liquid-phase DME production pathway *via* methyl formate (MF), discussing its potential advantages and current limitations, particularly related to low conversion rates.

1. Introduction

The changes in climate and different forms of environmental degradation represent some of the most pressing challenges of our era. The United Nations Climate Change Conferences, along with the Intergovernmental Panel on Climate Change (IPCC), urged to cut carbon dioxide (CO_2) emissions by at least 50% of current levels until 2050, setting a maximum of 2 °C as the acceptable global warming rate.[1–3] The primary sources of CO_2 emissions are transportation, industrial activities, and power plants, all of which are expected to increase in the coming years due to the rising energy demand. In response, various strategies and technologies have been developed over the past few decades to capture and store CO_2 (CCS). CCS is now considered a potential solution for reducing atmospheric CO_2 concentrations. Numerous research initiatives have been conducted globally, with CCS techniques categorized into geological CO_2 storage, ocean storage, and CO_2 mineralization into inorganic carbonates. Looking ahead, efforts to reduce CO_2 emissions will focus on improving CCS technologies and explore novel strategies for CO_2 recycling into energy carriers and chemical intermediates.

In this context, the CO_2-to-DME conversion has garnered considerable attention, as DME can serve as an intermediate for producing various value-added products or as an alternative fuel, as discussed further below.[3] DME is a promising fuel due to its ease of liquefaction at pressures above 5 MPa and its high energy density. Additionally, the direct synthesis of DME from CO_2 is thermodynamically more favorable than methanol synthesis, as it operates at lower pressures.[4] DME is non-toxic and environmentally benign, which has led to increased interest from both academia and industry. As a clean fuel, DME is attractive due to its simple molecular structure, consisting of only C–H and C–O bonds, without any C–C bonds. Its high oxygen content results in low particulate matter and CO formation when used as fuel.[5] DME shares similar physicochemical properties with liquefied petroleum gas (LPG), making it a potential substitute.[6] Table 1 refers to DME and diesel fuel's key properties and combustion characteristics.

DME's favourable properties, including its potential as a substitute for liquefied petroleum gas (LPG) and liquefied natural gas (LNG) in power plants, as well as its viability as an alternative to diesel fuel in vehicles, position DME as a

[a] *Leibniz Institute for Catalysis (LIKAT), Albert-Einstein-Str. 29a, D-18059 Rostock, Germany. E-mail: elka.kraleva@catalysis.de*
[b] *Biological, Chemical and Pharmaceutical Science and Technology (STEBICEF), Department, University of Palermo, Viale delle Scienze, Bld. 17, 90128 Palermo, Italy*
[c] *Department of Materials Engineering Science Graduate School of Engineering Science, Osaka University, 1-3 Machikaneyama, Toyonaka, Osaka 560-8531, Japan*
[d] *Institute of Physical Chemistry Polish Academy of Sciences, 01-224 Warsaw, Poland. E-mail: ipieta@ichf.edu.pl*

Table 1 Properties of DME and diesel fuel

Properties	DME	Diesel fuel
Molar mass, g mol^{-1}	46	170
Density (liquid), kg m^{-3}	667	831
Cetane number	>55	40–50
Auto-ignition temperature, K	508	523
Boiling point,[1] K	248.1	450–643
Enthalpy of vaporization, kJ kg^{-1}	467.13	300
Lower heating value, MJ kg^{-1}	27.6	42.5
Vapor pressure,[2] kPa	530	≪10

promising candidate for future high-performance fuel. As an alternative energy source, DME can address critical issues such as energy security, conservation, environmental sustainability, and the depletion of oil reserves. Notably, these challenges can be effectively mitigated using existing commercial technologies (*e.g.*, compression-ignition direct injection (CIDI) and hybrid systems), which offer a cost-effective solution that does not rely on uncertain future technologies with unpredictable timelines. As fuel processors and fuel cells are integrated into public transportation, DME can be further promoted as a non-toxic, non-corrosive, and environmentally friendly hydrogen carrier that can be produced from domestic resources. Thus, DME represents a versatile, low-carbon fuel suitable for the 21st century.[7,8]

The synthesis of DME can be accomplished *via* two primary methods: a one-step (direct) and a two-step (indirect) process.[9,10] In the conventional indirect synthesis, methanol is first produced from syngas (Fig. 1) using a metallic copper-based heterogeneous catalyst, typically $Cu/ZnO/Al_2O_3$, in the initial step through CO and/or CO_2 hydrogenation. However, this reaction is thermodynamically limited at high temperatures.[9] In the second step, methanol undergoes dehydration to form DME, facilitated by solid acid catalysts such as alumina, zeolites, or mixed metal oxides.

The direct DME synthesis from CO_2 presents the most promising option, as it utilizes CO_2 as a feedstock for producing DME, a highly valuable product. This process is more economical, as all reactions occur concurrently under milder operating conditions.[9,10] However, the direct synthesis of DME from CO_2 has not yet been extensively explored.

Conversely, the direct synthesis of DME from syngas offers an attractive alternative to the two-step process, as each product formed in the reaction can serve as a reactant for the subsequent step.[11] For instance, H_2 produced in the water–gas shift (WGS) reaction acts as a reactant for methanol synthesis. In direct DME synthesis, methanol formation and *in situ* dehydration co-occur, facilitated by hybrid catalysts in a single reactor (Fig. 2). This approach establishes more favorable thermodynamic conditions for methanol synthesis, leading to higher CO conversion and improved DME selectivity.[12–14] As a result, the overall reaction for direct DME synthesis is outlined in Fig. 2. Moreover, this process enables higher single-pass syngas conversion and lower H_2 demand (ideally with a reduced H_2/CO ratio), offering significant economic advantages and enhancing the industrial appeal of direct DME synthesis from syngas. Furthermore, process intensification within a single reactor, without the need for methanol separation units, can potentially lower both capital and operational costs for DME production.[15] However, in direct synthesis, methanol synthesis, dehydration, and the WGS reaction may occur concurrently. Ultimately, the success of these assumptions is contingent upon developing efficient and stable catalysts.

The indirect method of DME synthesis from syngas is well-established in industry; however, it is associated with significant drawbacks. This method leads to the release of CO_2, contributing to the GHG effect, and requires methanol dehydration, which thermodynamically disadvantages the overall process.[16–18]

The interest in the direct (one-step) route for DME synthesis is due to several major advantages, namely:

- *Thermodynamic benefits*: performing methanol dehydration *in situ* (Fig. 2) within the same reactor shifts the

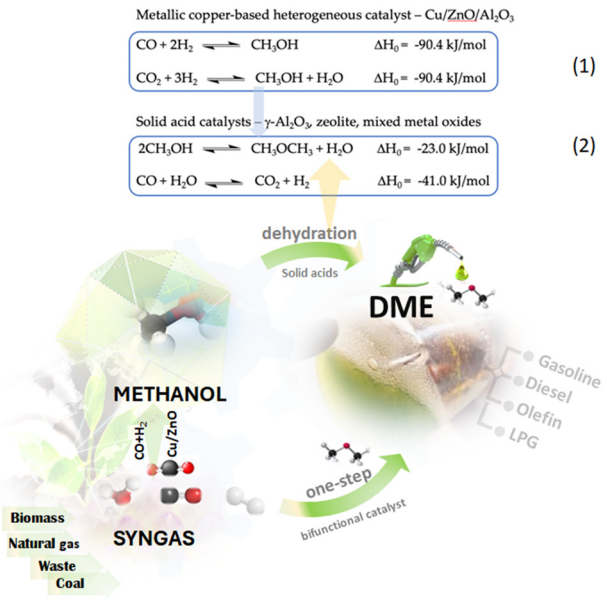

Fig. 1 Conventional (indirect) two-step process of DME synthesis from syngas.

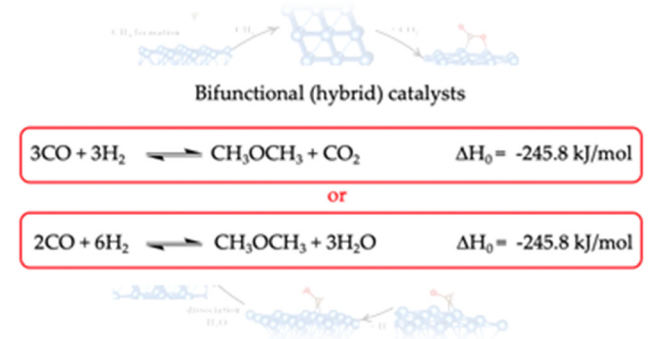

Fig. 2 Alternative (direct) one-step process DME synthesis.

equilibrium of methanol formation reactions, enhancing overall conversion efficiency.

• *Lower production costs*: compared to the two-step DME synthesis or standalone methanol synthesis, the direct process is more cost-effective. For a plant capacity of 2500 equivalent tons/day, the energy efficiency of direct DME synthesis reaches 64–68%, with energy demand reduced by about 5% and capital costs approximately 8% lower.[19]

• *Feedstock flexibility*: the process can utilize synthesis gas derived from a wide range of hydrocarbon-based feedstocks —including coal, natural gas, biomass, municipal waste, and even industrial off-gases such as mixtures of coke oven gas and tail gas from steel plants.

• *Support for biomass utilization*: the process encourages biomass gasification and anaerobic digestion, contributing to a carbon-neutral energy cycle.

• *Techno-economic advantages*: a comparative exergy-economic analysis of direct *versus* indirect DME synthesis (based on air–steam biomass gasification with CO_2) showed that the direct route had a lower production cost ($1.66 per kg *vs.* $2.26 per kg), lower energy consumption, and reduced net CO_2 emissions.[15] Moreover, the gasification-to-DME pathway from biomass was found to be ~7% more economically viable than the gasification-to-methanol route due to the higher market value of DME.[20]

• *Profitability from natural gas*: integrating DME synthesis with natural gas valorization can increase operational profitability.

Given these advantages, Olah *et al.*[21] identified the one-step DME synthesis as a key large-scale route for the catalytic valorization of CO_2. They also emphasized its sustainability, particularly when CO_2 is co-fed with syngas produced from lignocellulosic biomass.

Most studies on the direct synthesis of DME from syngas have focused on the impact of catalyst properties and reaction conditions (pressure, temperature, and gas hourly space velocity) using CO_2-free or low-CO_2 syngas. The presence of CO_2 is known to influence catalyst performance strongly. It is widely accepted that a small fraction of CO_2 in the syngas mixture is necessary to achieve a high methanol production rate; without it, catalyst activity tends to decrease due to excessive reduction of metal particles.[19–25] However, it has been determined that the optimal CO_2 concentration is only 2.4 vol%.[22,23] When syngas is produced from biomass or organic waste, the CO_2 content can be significantly higher than that of CO, depending on the type of biomass and the gasification process.[14,26–35] This deviation from the ideal CO_2/CO ratio for methanol synthesis may negatively impact DME yield in direct synthesis. Notably, most studies in the literature have used syngas mixtures with very low CO_2/CO ratios, close to the optimal for methanol production. Therefore, further experimental data on the direct synthesis of DME from syngas compositions with higher CO_2 content are essential for advancing DME synthesis from biomass-derived syngas.

Recently, an alternative liquid-phase DME synthesis pathway *via* methyl formate intermediates has been presented. This route offers potential for lower-temperature operation and simpler separation but is currently limited by low conversion rates and requires further development. Despite its early-stage status, it represents a promising direction in the broader context of CO_2 utilization.

To address these challenges and opportunities, this review provides a comprehensive overview of recent advances in CO_2-to-DME synthesis, encompassing both direct and indirect processes. We place particular emphasis on: (1) thermodynamic and kinetic considerations affecting CO_2 hydrogenation, (2) catalyst design for both methanol synthesis and methanol dehydration, (3) integrated bifunctional catalyst systems for one-step processes, (4) emerging liquid-phase DME synthesis routes, including the methyl formate pathway, and (5) process intensification strategies aimed at improving conversion efficiency and reducing energy input.

Through this analysis, we aim to provide a clearer understanding of how advanced catalysts and reactor configurations can enable scalable, low-carbon DME production from CO_2. Special attention is devoted to the synergy between redox and acid functions in bifunctional catalysts—an area of active research with critical implications for catalytic performance. While gas-phase direct synthesis remains an attractive one-step route, the development of innovative liquid-phase processes presents new opportunities to reduce operating costs and energy demands, offering a complementary and potentially transformative approach to CO_2 valorisation.

2. Current status of CO_2 to DME transformation and thermodynamic challenges

The direct CO_2-to-DME represents a crucial alternative process for green DME production, necessitating a more thorough thermodynamic analysis. Key factors influencing this process include temperature, pressure, the $H_2/CO_2/CO$ ratio, and water (H_2O) formation.[22] To evaluate the impact of these factors on DME yield during direct synthesis, the thermodynamics of the reaction have been studied in several publications.[23–27] The Gibbs free energy minimization method, applied using Aspen Plus® software, is commonly employed to analyze the equilibrium composition of reforming systems. Given the complexity of the reaction network, which involves the formation of multiple products, it is essential to include all relevant species in the modeling and analysis.

According to reaction mechanism analysis, the main products considered in these studies include CO_2, H_2, CO, H_2O, methanol (MeOH), and DME, which correspond to the key reactions in the system. One noteworthy study by Hankin *et al.*[28] re-examined and compared the

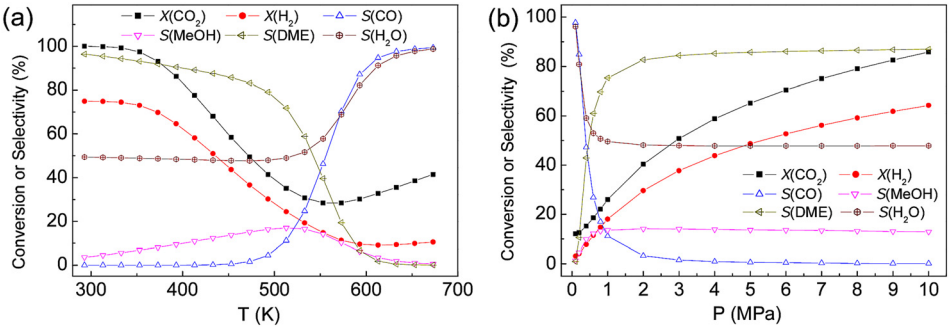

Fig. 3 Effects of (a) temperature at 3.0 MPa and H_2/CO_2 = 4 and (b) pressure at 473 K and H_2/CO_2 = 4 on the equilibrium product distribution in CO_2 hydrogenation to DME (X = conversion; S_i = selectivity to product) copyright[29] 2017 Earth and Environmental Science.

thermodynamic constraints of methanol and DME synthesis from CO- and CO_2-based syngas using system analysis with Aspen Plus V8.8. The primary research question addressed whether CO_2 could be directly fed into the methanol/DME synthesis process or if upstream conversion to CO *via* the reverse water–gas shift (RWGS) reaction was necessary. Consequently, the study investigated process efficiency and expected CO_2 conversion in four methanol/DME synthesis variants as a function of the feedstock's $H_2/(CO_2 + CO)$ and CO_2/CO ratios. These investigations revealed that the highest efficiency for methanol, direct DME, and two-step DME processes was achieved with a non-stoichiometric H_2/CO_2 ratio of 2.5, without upstream CO generation. For CO-based syngas, optimal methanol, two-step DME, and direct DME synthesis efficiencies were obtained at stoichiometric H_2/CO feed ratios of 2 and 1, respectively. Direct CO_2 recovery is only feasible when maximum energy savings are achieved.

2.1 Effects of temperature and pressure

Temperature and pressure significantly affect the equilibrium distribution of products in the hydrogenation of CO_2 to DME (Fig. 3a and b). As the reaction temperature increases, the equilibrium conversion of CO_2 initially decreases from 100%, reaching a minimum (Fig. 3a), primarily due to water (H_2O) formation and the reverse water–gas shift (RWGS) reaction. Although methanol (MeOH) selectivity reaches a maximum ~540 K, it does not become the predominant product throughout the process. Concurrently, DME selectivity declines with reduced MeOH formation, increasing H_2O content, and the competing RWGS reaction that generates CO at higher temperatures.[29] These trends can be attributed to the exothermic nature of CO_2 hydrogenation to MeOH and DME, coupled with the endothermic nature of the RWGS, which accelerates at elevated temperatures, thereby shifting the product distribution towards CO.

In contrast, high pressure enhances the conversion of CO_2 and H_2, as well as the selectivity for both DME and MeOH, while having a minimal effect on CO selectivity (Fig. 3b).

The overall reaction equation ($2CO_2 + 6H_2 \rightleftharpoons$ DME + $3H_2O$) indicates that the target reaction reduces the total number of moles, favoring the formation of the desired products.

Based on the aforementioned analysis and economic considerations, it is recommended that the typical CO_2 hydrogenation process for DME synthesis should operate at low temperatures (<600 K) and high pressures (2–6 MPa). This conclusion aligns with findings from several relevant studies.[23–26] Therefore, the DME synthesis process requires industrial catalysts with high activity at low temperatures.[30] Additionally, these catalysts must be capable of handling the high concentrations of water (H_2O) expected to be formed during the reaction.[29]

2.2 Effect of H_2/CO_2 molar ratio

Fig. 4 illustrates the effect of the H_2/CO_2 molar ratio on the equilibrium product distribution in the CO_2 hydrogenation process to DME. As the H_2/CO_2 ratio increases, CO_2 conversion and DME selectivity rise, while CO selectivity experiences a slight decline. The selectivity for methanol remains unaffected by H_2/CO_2 ratio changes. These results suggest that a higher H_2/CO_2 molar ratio is favorable for the hydrogenation process. However, when the $H_2/(CO + CO_2)$

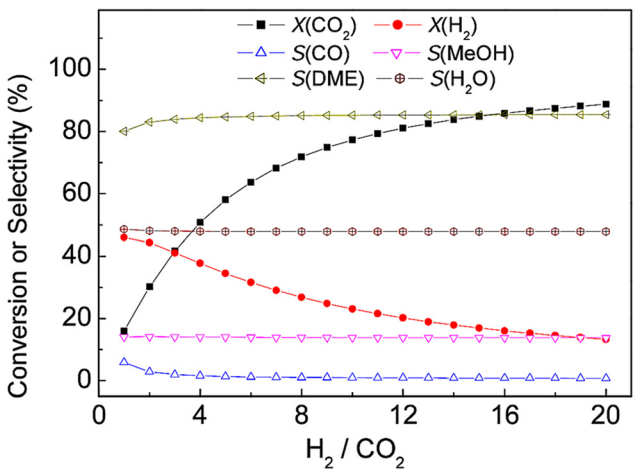

Fig. 4 Effect of H_2/CO_2 molar ratio on equilibrium product distribution in CO_2 hydrogenation to DME. Reaction conditions: 473 K, 3.0 MPa copyright[29] 2017 Earth and Environmental Science.

ratio is increased to 5, the increase in DME selectivity with the H_2/CO_2 ratio becomes slower. To optimize H_2 usage and achieve high CO_2 conversion and DME selectivity, the process should be operated below 550 K, with the H_2/CO_2 ratio maintained between 3 and 6.[29]

2.3 Effects of adding H_2O or CO to feed

Fig. 5 illustrates the calculated effect of H_2O or CO admixture in the feed on the equilibrium product distribution in CO_2 hydrogenation to DME. Due to equilibrium limitations, the incomplete conversion of H_2 and CO_x in the process necessitates the recycling of residual feed components after the separation of target products. These components, primarily H_2, CO, and CO_2, can impact both reaction kinetics and chemical equilibrium.[29]

The conversion of CO_2 and the selectivity for DME decrease as the amount of H_2O in the feed decreases, while CO and methanol selectivity increase (Fig. 5a). This behavior is primarily because water favors reverse reactions; thus, it is necessary to remove the generated water continuously during the process. Fig. 5b shows the calculated effect of CO addition on the equilibrium product distribution. The conversion of H_2 increases with the CO/CO_2 ratio. When CO is added to the feed, the water–gas shift (WGS) reaction may occur, increasing DME's equilibrium yield. This is because increasing the CO content effectively removes part of the water, driving methanol synthesis in the forward direction, which slightly reduces the equilibrium yields of DME and H_2O. However, when the amount of CO in the feed exceeds that of CO_2, the process shifts towards CO hydrogenation, facilitating DME formation.

From a thermodynamic perspective, low temperature and high pressure are advantageous for CO_2 hydrogenation to DME. Thermodynamic optimization suggests the optimal conditions for high conversion and high DME selectivity are a temperature below 550 K, a pressure range of 2–6 MPa, and an H_2/CO_2 ratio of 3–6. Adding CO benefits CO_2 hydrogenation to DME, while additional H_2O is detrimental to the reaction and should be removed as much as possible.[29]

These studies highlight the thermodynamic advantages of CO_2 hydrogenation to DME by coupling CO_2 hydrogenation with methanol dehydration, although achieving complete conversion of methanol to DME remains unfeasible. As mentioned earlier, direct DME synthesis from CO_2 is favored under high-pressure and low-temperature conditions. However, operating at low temperatures necessitates optimizing reactor designs and innovations such as *in situ* water removal (*via* distillation, adsorption, or membranes)[31,32] or developing more active CO_2 hydrogenation catalysts.

3. Catalysts for direct gas phase DME synthesis

3.1 Catalysts functionality: metallic and acid sites

An effective catalyst for the direct synthesis of dimethyl ether (DME) must integrate both metallic sites—to facilitate methanol formation from CO_2 and H_2—and acidic sites for the subsequent dehydration of methanol to DME, ideally within a single bifunctional system. Key design parameters include the incorporation of highly active and stable metal centres capable of activating CO_2 and H_2 under mild conditions, and the homogeneous dispersion of both metal and acid sites to minimize diffusion limitations and enhance reaction rates.[33,34] The acidity must be carefully tuned: sufficient to promote methanol dehydration but not so strong as to induce undesirable side reactions or coke formation. Additionally, tailored porosity and nanostructuring can improve mass transport and accessibility to active sites. Importantly, hydrophobic surface properties are increasingly recognized as critical for maintaining catalytic stability by mitigating water adsorption and accumulation, which can lead to deactivation through site poisoning or support degradation.[33,35]

CuO/ZnO catalysts with various additives are primarily used to provide metallic functions, while zeolites or γ-Al_2O_3 are commonly used to introduce acidic sites. In commercial methanol production from syngas, the $CuO/ZnO/Al_2O_3$ catalyst is employed, with operating temperatures of 250–280 °C and pressures of 6–8 MPa.[36–41] The effects of active components have been reported,[37] along with the influence

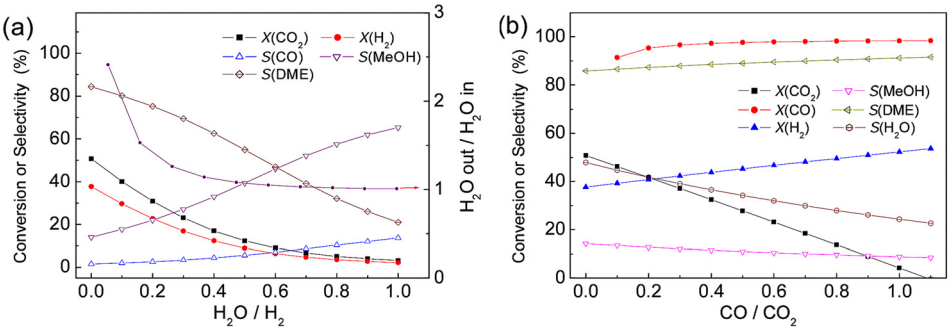

Fig. 5 Effect of a) H_2O or b) CO addition to feed on equilibrium product distribution in CO_2 hydrogenation to DME. Reaction conditions: 473 K, 3 MPa, H_2/CO_2 = 4. Copyright[29] 2017 Earth and Environmental Science.

Table 2 Catalysts for DME synthesis with different active metal sites

Catalyst system	Catalyst compositions	Key functions	Performance highlights	Ref.
Cu-based (CZA)	$CuO–ZnO–Al_2O_3$	Cu^0/Cu^+: active species; ZnO: dispersion/stability; Al_2O_3: structural support	Classic benchmark catalyst; limited stability under harsh conditions	
$Cu–ZnO–ZrO_2$	Cu^0/Cu^+ + ZnO + ZrO_2	ZrO_2 stabilizes $Cu^{\delta+}$, increases oxygen vacancies, improves H_2O tolerance, boosts CO_2 adsorption	High MeOH selectivity & CO_2 conversion (*e.g.* 8.14%, MeOH >98%); optimized Cu/Zn/Zr = 2 : 1 : 1	44–47
Cu–ZnO–MnO	Cu^0/Cu^+ + MnO	Enhances CuO/ZnO dispersion, increases active surface area, improves WGS reaction	Boosts DME yield; low-cost alternative to CZA	48, 49
$Cu–ZnO–Ga_2O_3$	Ga_2O_3 as promoter	Improves reducibility, Cu stability & dispersion; enhances ZnO conductivity; introduces redox-active defect sites	Achieves high MeOH yields	50–53
$Cu–ZnO–TiO_2$	TiO_2 as promoter	Generates oxygen vacancies for CO_2 activation	Enhanced activity; part of quaternary systems	54
$Cu–ZnO–Al_2O_3–CeO_2$	CeO_2 as promoter	Improves oxygen mobility, suppresses rWGS reaction	Good activity and stability	55, 56
Cu–ZnO + noble metals	Au, Pd, Pt, Rh (trace amounts)	Hydrogen spill-over enhances H_2 activation	Boosted activity & MeOH production	57–63
In_2O_3 and $In_2O_3–ZrO_2$	In_2O_3, ZrO_2	Oxygen vacancies as active sites; Zr doping increases surface defects	Stable up to 1000 h TOS; excellent MeOH selectivity, rWGS suppressed	64–70
$In_2O_3–Ga_2O_3$	Ga doping	Creates additional surface defects, enhances CO_2 activation	Improved performance when In/Ga ratio optimized	67
$ZnO–ZrO_2$ (non-Cu)	$ZnO–ZrO_2$	Zn–O sites active for H_2 activation and direct CO_2 hydrogenation	High CO_2 conversion, excellent stability (~500 h)	71
Mn–Co-based	Mn + Co	Synergy increases basicity; inhibits rWGS; improves MeOH selectivity	Promising for CO_2 hydrogenation	72–74
$Pd/CeO_2–Ca$	Pd nanoparticles (2–6 nm), Ca-doped CeO_2	Ca induces CeO_2 defects, balances acidity/basicity, Pd^0 stable	Active for MeOH synthesis and DME dehydration; enhanced CO_2 adsorption	75
Pd–Zn alloys	Pd + Zn	Stabilizes formate intermediates; inhibits CO formation	Efficient MeOH synthesis *via* CO_2 pathway	76, 77
Au-supported catalysts	Au/ZnO, Au/ZrO_2, Au/TiO_2, Au/Al_2O_3	Activity/selectivity depend on support and particle size	Au/ZnO best selectivity; large Au particles → lower activity; operates *via* direct CO_2 hydrogenation	78–80
Au/ZrO_2	Au (sub-nanometric), ZrO_2	Strong metal–support interaction; improved dispersion	High MeOH selectivity and stability	81

of supports,[38,39] promoters,[40] preparation methods,[41] and calcination temperatures[36] on the CO_2-to-DME direct synthesis. Significant efforts have been made, particularly with respect to long-term stability; however, DME yield remains limited. As a result, the number of studies focusing on CO_2 hydrogenation to DME is still lower compared to those on CO hydrogenation to DME.[42]

To critically assess the catalytic progress in CO_2-to-DME and CO_2-to-methanol synthesis, Table 2 compares representative catalyst systems based on their compositions, key functionalities, and reported performance metrics. Systems incorporating ZrO_2 and Ga_2O_3 consistently demonstrate higher CO_2 conversion and MeOH selectivity due to enhanced oxygen vacancy formation and improved Cu

Table 3 Most studied acid catalysts for methanol dehydration to DME

Catalyst	Key features	Challenges	Modifications	Ref.
HZSM-5	High activity, good hydrothermal stability, well-studied	Strong Brønsted acidity, respectively coke formation	Desilication, dealumination, silication, hlorination/fluorination, mesoporous structuring, nanostructuring to reduce acidity and coke	83–85
SAPO-11	Weak acid sites, good DME selectivity, high hydrothermal stability	Moderate activity	Nano-sized SAPO-11 (~200 nm) increases surface area and mesoporosity; better than SAPO-18 and HZSM-5	45, 86
MCM-41 + TPA	High TOF for methanol dehydration	Limited hydrothermal stability	Used as a support for tungstophosphoric acid (TPA)	87
Other zeolites (BEA, FER, MOR, *etc.*)	Tunable framework, porosity, and acidity	Varies by type	FER and MFI shown to perform well in terms of selectivity and stability	88, 89
Ferrierite (FER)	Moderate acidity, good pore structure	Less studied than MFI-type	Exhibits optimal performance due to balance of acidity and structure	90, 91

dispersion.[43] However, discrepancies in reported productivity and lack of standardized testing protocols remain a challenge. Further benchmarking under comparable conditions is needed to draw definitive conclusions on long-term stability and industrial viability.

In most studies, γ-Al_2O_3 is used as an acidic catalyst for methanol dehydration into DME, given its reported high selectivity within the temperature range required in the process (200–300 °C) and relatively low manufacturing.[37,82] Last research was focused on the zeolites as solid-acid catalysts for methanol dehydration to DME. The main used materials and them properties are summarized in Table 3.

Combinations of CuO–ZnO materials with various types of zeolites, such as the H-form of FER-type, H-Mordenite, SAPO-11, H-Beta, and MFI-type zeolites, prepared with varying Si/Al ratios, have been extensively investigated to identify a catalytic system that exhibits high activity, selectivity, and stability.[24,54–57,64] The zeolite structure, the characteristics of the Lewis and Brønsted acid sites, and the Si/Al ratio significantly influence the dehydration of methanol to DME. Frusteri *et al.*[49,87,91–94] examined the role of acid sites in hybrid catalysts prepared by gel-oxalate precipitation of CuZnZr precursors onto ZSM-5 crystals with a Si/Al ratio within a specific range. Their findings suggest that the

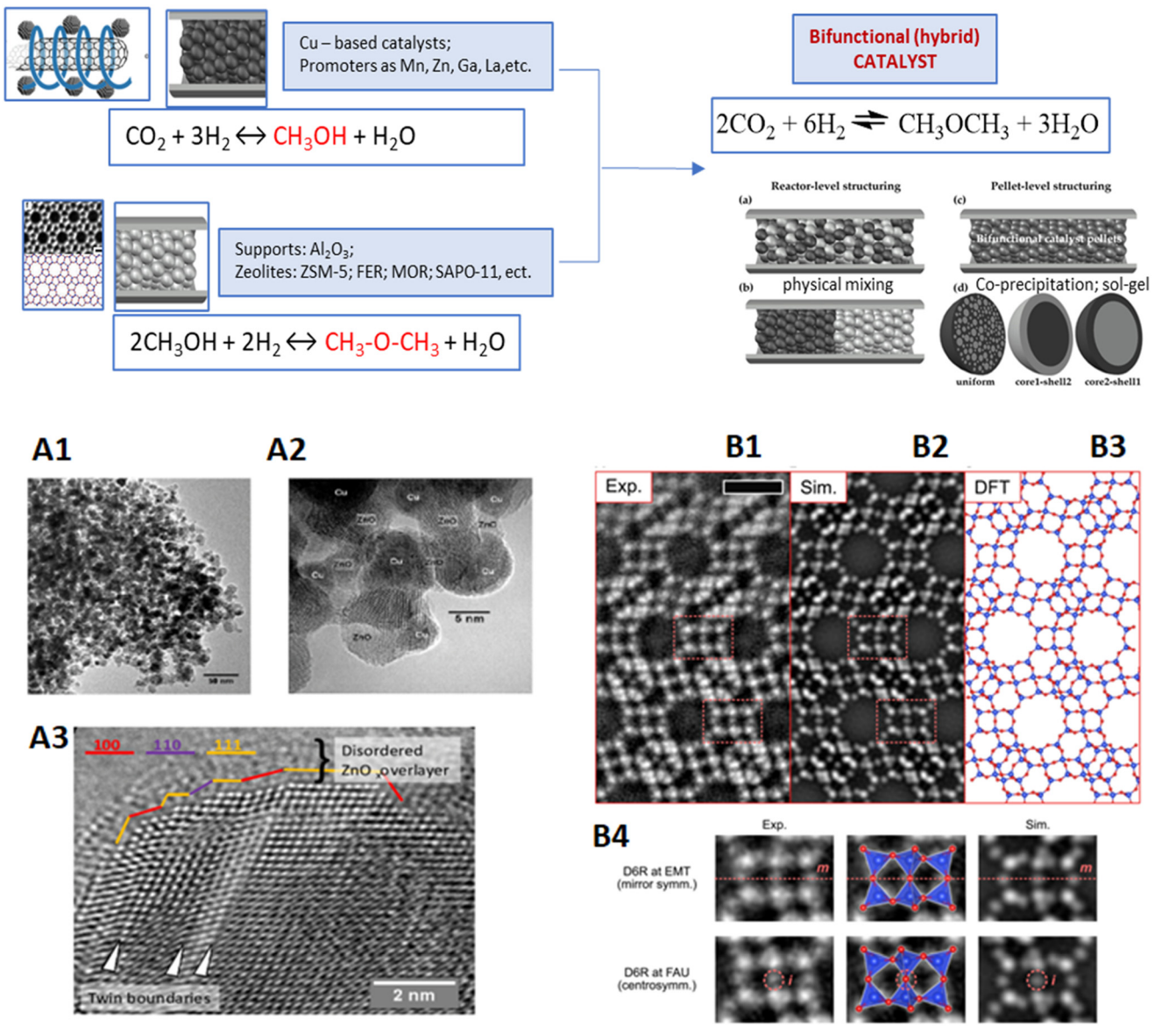

Fig. 6 Studied designed catalysts for DME synthesis. Conventional catalysts for DME synthesis from syngas. A – HRTEM images of a Cu/ZnO/Al_2O; A1 – porous aggregates of metallic Cu and ZnO, A2 – Cu/ZnO/Al_2O_3 nanoparticles, A3 – details of the surface faceting, decoration, and defect structure, B – OBF STEM images of a zeolite catalysts: B1 – unit-cell-averaged experimental OBF image. Scale bar, 1 nm. B2 – Simulated OBF image based on the DFT-relaxed structure shown in B3. B3 – Atomic structure model of FAU twin boundary relaxed by the DFT calculation. The blue and red balls indicate the *T* and oxygen sites, respectively. B4 – Comparison of D6R structures on the twin boundary and bulk region. Experimental and simulated images are shown for each structure, and atomic structure models represented as a TO_4 tetrahedral configuration are overlaid. Copyright[137,138] 2017 Earth and Environmental Science.

acidity of the zeolite must be carefully controlled to balance catalytic activity and resistance to deactivation by water. Furthermore, the authors demonstrated that ZSM-5 with a high Si/Al ratio exhibited excellent water resistance but low activity for methanol dehydration.[57–64] In contrast, more acidic ZSM-5 samples with a lower Si/Al ratio displayed high methanol conversion but poor water resistance and low DME selectivity. The ZSM-5 zeolite with a Si/Al ratio of 38 showed optimal properties in terms of CO_2 conversion, DME yield, and water resistance.[87–95] The addition of water to the feed resulted in only a minor reduction in methanol conversion over ferrierites, whereas γ-Al_2O_3 exhibited considerable inhibition. Moreover, FER-type zeolites demonstrated a reduced tendency to form coke when water was co-fed with methanol.[92] Regardless of the catalyst modification method or contact time, the methanol conversion and DME selectivity over all discussed CuO–ZnO materials with different types of zeolite catalysts were consistently 100% at temperatures of 200 and 225 °C.

For the direct hydrogenation reaction of CO_2 to DME, zeolites are particularly advantageous due to their acidic properties, negligible sensitivity to water, shape selectivity, and high specific surface area.[26,93–109] Copper is the most commonly used active metallic phase in combination with zeolites, although its performance is often unsatisfactory. Consequently, many researchers incorporate additional metallic phases, such as zinc, zirconium, lanthanum, cerium, and aluminum, in the form of oxide precursors.[93–104] CuO combined with TiO_2 and ZrO_2 mixed oxides and HZSM-5 has also been investigated for direct DME synthesis.[110] The best catalytic performance was achieved with a Ti/Zr atomic ratio of 1, resulting in approximately 16% CO_2 conversion and 48% DME selectivity.

Zhou *et al.*[30] demonstrated that the addition of CeO_2 to a CuO–Fe_2O_3 catalyst increased both the quantity of Lewis and Brønsted acid sites and the acid strength of the weak acid sites, thereby enhancing the catalytic performance in CO_2 hydrogenation to DME. A CuO–Fe_2O_3–CeO_2/HZSM-5 catalyst containing 3.0 wt% CeO_2 achieved 20.9% CO_2 conversion and 63.1% DME selectivity at 260 °C and 3.0 MPa. Qin *et al.*[27] evaluated bifunctional Cu–Fe/HZSM-5 catalysts doped with 1 wt% lanthanum or cerium at 3 MPa and 260 °C. Their results confirmed that cerium doping had a more significant effect on the Cu crystallite size, reducibility of Cu, and specific surface area compared to lanthanum. The Ce-doped Cu–Fe–Ce/HZSM-5 catalyst showed a 50% improvement in CO_2 conversion relative to the undoped bifunctional catalyst, with nearly 100% DME selectivity. Both doped catalysts exhibited stable performance over 15 hours.

3.2 Catalyst design and preparation

To prepare the active catalyst for direct hydrogenation of CO_2 to DME, metal functions (Table 2) and acid functions (Table 3) must be combined, usually with an excess of acid sites in bifunctional or hybrid systems. The two types of catalysts differ in the contact between the acid and metal sites: bifunctional catalysts have separate metal and acid sites, whereas in hybrid catalysts there is direct contact between them. The control of the contact between the metal and acid sites is one of the key factors determining the catalyst efficiency for direct DME production.[111,112]

One approach to optimizing the properties of multifunctional catalysts is improving the preparation procedure. Various strategies have been employed to prepare bifunctional catalysts for direct DME synthesis. The general process for preparing bifunctional catalysts is illustrated in Fig. 6. One of the simplest methods for preparing hybrid catalysts is the physical or mechanical mixing of the methanol synthesis catalyst (metal function) with the solid acid catalyst. A key characteristic of the physically mixed hybrid catalyst is that both functions—methanol synthesis and methanol dehydration—exist independently before the mixing process. The arrangement of these catalysts within a reactor plays a substantial role in determining catalytic performance.[21]

In contrast, more complex one-pot synthesis methods using chemical techniques, such as co-precipitation (sol–gel), sequential precipitation, chemical metal deposition, and sonochemical-assisted impregnation, enable more intimate mixing of the components and produce hybrid catalysts with superior performance. Regardless of the preparation method used, the goal remains the same: to control the dispersion of the active phases (metal and acid) and optimize the contact between metal and acid sites.

A list of well-known physically mixed hybrid catalysts, specifically for one-pot CO_2 hydrogenation to DME, is provided in Table 4.[93–99]

Li *et al.*[100] explored the impact of three different mixing methods for CuO/ZnO/Al_2O_3 (CZA) + HZSM-5 bifunctional catalysts on stability in DME synthesis from CO_2. While initial CO_2 conversion and DME yield were unaffected by mixing methods, long-term tests revealed that the mixing method significantly impacted catalyst stability. The contact between Cu active sites and HZSM-5 was found to influence Cu oxidation. Severe Cu oxidation and metal ion migration to

Table 4 Physically mixed hybrid catalysts for one-pot CO_2-to-DME process. T = reaction temperature, p = reaction pressure; X% CO_2 = conversion of CO_2; S_i% = selectivity to i product[57–114]

Catalysts	T (°C)	P (bar)	X% CO_2	S_i% selectivity of i-products			
				MeOH	DME	CO	CH_4
Cu/Zn/Al–γ-Al_2O_3	260	50	15	15	3	82	—
Cu/Zn/Al–HZSM-5	260	50	29	2	65	33	—
Cu/Ti/Zr–HZSM-5	275	30	16	13	47.5	39.2	—
Cu/Fe/Ce–HZSM-5	220	30	21	5	63.2	25	6
Cu/Fe/La–HZSM-5	260	30	40	—	100	—	—
Cu/Fe/Ce–HZSM-5	260	30	50	—	100	—	—
Cu/Zn/Zr–SAPO-11	275	30	9	17	80	8	—
Cu/Fe/Zr–HZSM-5	260	30	29	15	65	8	13
Cu/Zn/Al–ZSM5 + CNTs	260	30	46.2	35.6	45.2	19	—

HZSM-5 led to reduced acidic sites due to the high water generated in CO_2 hydrogenation.

3.3 Catalytic bed configuration

The arrangement of the catalytic bed in the reactor affects catalyst selectivity.[113] Higher DME yields have been observed when both functions are integrated into a single fixed-bed reactor, compared to using spatially segregated catalysts in two fixed beds.[92,114] Each configuration of the catalyst system presents distinct characteristics and uniquely influences catalytic performance.

Several catalyst arrangements have been investigated in the literature and we present it in Table 5.

3.4 Alternative advanced catalysts

The ability to spatially organize different active sites at the nanoscale significantly advance the development and optimization of emerging multifunctional catalysts. In this context, hierarchical structures, where various building blocks are arranged with nano-scale precision, can interact synergistically, leading to enhanced catalytic properties that are unattainable when considering the individual components in isolation. This approach entails expanding surface areas and precisely designing surface-active sites, particularly those responsible for CO_2 adsorption and product formation. Advanced topologies, such as hollow and/or porous structures, as well as low-dimensional nanomaterials (*e.g.*, quantum dots, nanorods, nanowires, nanotubes, nanosheets, nanoplates, and nanodiscs), can provide a higher density of active surface sites.[108] Furthermore, nano-scale structures enhance charge transfer to surface adsorbates by minimizing the migration distance.

Spinels. At the laboratory scale, $CuO–ZnO–Al_2O_3$ (CZA) catalysts have been predominantly utilized due to their commercial relevance in methanol synthesis, providing metallic functionality. Recent innovations have focused on the CuM_2O_4 (M = Fe, Mn, Cr, Ga, Al, *etc.*) spinels usage with $CuFe_2O_4$ garnering significant attention due to its excellent thermal stability,[115,116] which enables it to recover its activity during reaction–regeneration cycles.[117,118] Initially, γ-Al_2O_3 was the most commonly used acidic material for DME synthesis,[119,120] but it has since been gradually replaced by more active HZSM-5. To avoid the formation of hydrocarbons and coke, HZSM-5 requires appropriate treatment, such as desilication *via* alkaline treatment.[121] In parallel, Oar-Arteta *et al.*[117] have improved the properties of γ-Al_2O_3 through optimal calcination of pseudo-boehmite, resulting in a catalyst with high mechanical strength (a deficiency observed in $CuFe_2O_4$ spinels) and moderate acidity, which helps minimize hydrocarbon formation. This modification enables stable operation during reaction–regeneration cycles at 350 °C, resulting in a DME yield of 82%.

Carbon nanostructures (CNF). A promising example of novel hybrid materials for DME synthesis includes carbon nanostructures (CNF) such as nanotubes, nano-horns, or graphene, which are coated with different metal oxide layers in which metal nanoparticles can be embedded. This approach has been successfully applied in heterogeneous thermo-, electro-, and photo-catalytic processes,[122–126] where co-axial heterostructures based on multi-walled carbon nanotubes have shown improved catalytic activity compared to the corresponding metal/oxide combinations without the inclusion of carbon nanomaterials. The enhanced performance is attributed to both the geometrical/morphological characteristics and the electronic properties of the resulting hybrids, as well as their homogeneous structure.

To achieve the desired CNF/inorganic hybrid materials, two general approaches can be pursued (Fig. 7): 1) the reaction of pristine or functionalized CNF with a metal oxide precursor to obtain covered CNF, which then serves as a support for either *in situ* formed or preformed metal nanoparticles (MNP); 2) the combination of preformed functionalized MNP with metal alkoxides to form core–shell structures, which are subsequently deposited onto the CNF surface, resulting in the formation of hybrid structures. By utilizing these strategies, several metal oxide layers, including TiO_2, Al_2O_3, SiO_2, CeO_2, and ZnO, among others, have been successfully deposited on CNF, providing support for nanoparticles such as Pd, Ru, Co, and Au.[127] This method represents an unexplored approach for the direct synthesis of

Table 5 Advanced configuration of the catalytic bed

Configuration type	Description	Impact on performance
Dual-bed configuration	Metallic catalyst bed (MeOH synthesis) placed before acidic bed (MeOH dehydration to DME)	Advantages: optimized for temperature gradient control and catalyst stability **Challenge**: methanol formed in the first layer can desorb before reaching the second, possibly reducing DME yield if not managed carefully. Lower activity due to intermediate MeOH diffusion
Physical mixture	Metallic and acidic catalyst particles physically mixed in one bed	Moderate performance: intimacy depends on mixing homogeneity
Structured catalyst	Catalysts coated on structured supports (*e.g.*, foams, monoliths, 3D-printed scaffolds) with organized distribution of functions	**Advantage**: enhanced mass/heat transfer, reduced pressure drop, tunable porosity **Application**: useful for high-throughput modular reactors, often compatible with microreactor systems. Promising for industrial applications and scalability of process

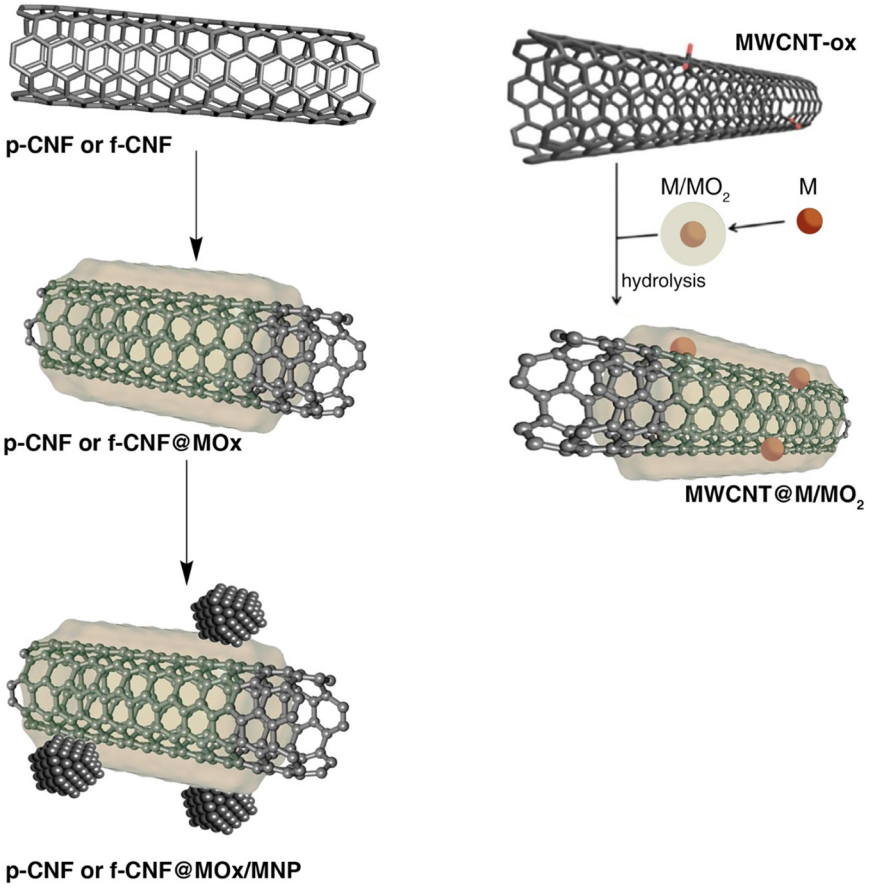

Fig. 7 Synthetic pathways for the preparation of CNF-based hybrid materials.

DME, potentially unveiling access to a variety of finely tuned materials with unique and unprecedented properties.

Mesoporous silica nanoparticles (MSN). Alternatively, mesoporous silica nanoparticles (MSN),[128,129] which possess honeycomb or hollow structures and offer both internal and external surface areas, have also emerged as a promising support material. These nanoparticles feature small pore sizes (2–3 nm), high surface areas, and substantial pore volumes.[130,131] The properties of MSN, including the parallel or radial pore organization achieved through the emulsion-condensation route, are influenced by sol preparation conditions such as pH and the molar ratio of components in the emulsion. In general, mesoporous silica is suitable for CO_2 capture due to its high specific surface area and large pore volume. However, certain limitations exist, including challenges with functionalization and irregular particle size distribution. To overcome these drawbacks, MSN can be functionalized with active compounds (*e.g.*, Zr, Al, Zn, phosphotungstic acid) or modified with specific moieties[132] that stabilize nanoparticles or facilitate the linking of metal complexes to enhance catalytic properties.[133,134] The size of the MSN can be tuned to control the uniform distribution of active species, thus optimizing catalytic performance,[135] as demonstrated in the case of palladium and gold nano-catalysts[82] and noble metal nanoparticles supported on MSN.[136] Additionally, the catalytic performance of MSN-supported materials has been demonstrated in processes such as the epoxidation of limonene,[137] and CO_2 capture.[138]

Understanding how parameters such as morphology and pore organization influence performance can significantly enhance the efficiency and sustainability of catalytic processes, particularly when compared to well-known micro-sized supports like MCM-41 or SBA-15.[134] To ensure effective synthesis, care must be taken to prevent the leaching of precursor complexes or the separation of functional sites. Synthetic routes using colloidal solutions, microemulsions, or micellar systems may prove beneficial in this regard.[139] Furthermore, process development should account for the economic considerations of solvent and surfactant removal, as well as the biodegradation of hydrophobic organic groups and surfactants (both ionic and neutral). Machine learning techniques may also offer valuable insights in evaluating catalyst performance, especially in relation to features, synthesis procedures, and types of supports, as has been demonstrated in several industries.[140]

Heteropolyacids. To overcome the limitations of zeolites in methanol dehydration, heteropolyacids (HPAs) supported on high surface materials (like TiO_2, SiO_2, ZrO_2) offer a promising alternative.[90–97,141] HPAs, such as $H_3PW_{12}O_{40}$ and $H_4SiW_{12}O_{40}$, have strong Brønsted acidity, pseudo-liquid

behavior, and operate at lower temperatures. Their structure allows for both surface and bulk dehydration of methanol. However, due to their low surface area, HPAs are often supported on oxides to improve dispersion and accessibility of acid sites. These supported systems have shown high activity and selectivity toward dimethyl ether (DME) and can outperform traditional zeolite-based catalysts in both methanol dehydration and CO_2 hydrogenation reactions. Optimal loading and support choice are key to maximizing performance and minimizing deactivation.

The study by Kornas *et al.*[141] examined the effect of the type of HPA ($H_3PW_{12}O_{40}$, HPW) and $H_3PMo_{12}O_{40}$ (HPMo) supported on montmorillonite K10 on the activity of the hybrid catalyst combined with CuO/ZrO_2 in the direct CO_2 hydrogenation to DME. Due to the higher acidity of HPW compared to HPMo, the HPW-modified catalyst proved to be more active and stable under the reaction conditions employed than its HPMo-modified counterpart. The acidity of the catalyst and its thermal stability were the main factors influencing the catalytic activity.[141]

Phosphotungstic and silicotungstic acid salts. Phosphotungstic and silicotungstic acid salts (CuPW, CuSiW, FePW, FeSiW) were also studied in the reaction of dehydration of methanol.[141–143] Copper salt catalysts showed a high DME selectivity (100%) at low temperature (100–250 °C), while the FeSiW and FePW salts showed similar DME selectivity at higher temperature (250 °C). The silicotungstic acid salts were most stable under the reaction conditions (120 h lifetime) than the phosphotungstic counterparts.

Metal nitrides. Metal nitrides represent a unique class of catalysts widely applied in processes such as the water–gas shift reaction, as well as CO and CO_2 hydrogenation, largely due to their distinct ligand interactions and ensemble effects.[144–146] Gallium-based materials, including Ga promoters and intermetallic gallium compounds, have shown notable effectiveness in converting CO_2 into methanol. Theoretical studies using density functional theory (DFT) also indicate that gallium nitride (GaN) possesses acidic characteristics.[145]

Building on these insights, Liu *et al.* conducted experiments showing that GaN can directly catalyze the hydrogenation of CO_2 to dimethyl ether (DME) under reaction conditions of 300–450 °C and 2 MPa.[145] Their study further explored the function of acidic sites on the catalyst, revealing that the addition of DME and water to the feed enhances methanol production. Unlike conventional hybrid systems, GaN favors the direct formation of DME as the primary product, with methanol appearing as a secondary product *via* DME hydrolysis. The Brønsted acid sites on GaN enhance methanol formation under certain conditions, and its activity is highly temperature- and pressure-dependent. This reversible acid behavior and distinct product pathway make GaN a promising alternative for DME synthesis from CO_2.[145]

Core–shell catalysts. Recently, catalysts with core–shell-like structures have been explored for DME synthesis.[42,106–108] These materials consist of a methanol synthesis catalyst at the core and a methanol dehydration catalyst at the shell. Methanol formed in the core diffuses outward, where it is converted into DME in the shell. Core–shell structured bifunctional catalysts have been developed to mitigate thermodynamic limitations by compartmentalizing the reaction steps within different regions of the material. This combination of functions within a single catalyst particle may generate synergies between the different catalytic processes.[42] Several core–shell catalysts, including Cr–ZnO/SAPO-46,[108] CuO–ZnO/HZSM-5,[98] Cr–ZnO–S/H-ZSM-5,[97] H-ZSM-5/Cu–ZnO–Al_2O_3,[147] CuO–ZnO–Al_2O_3/SiO_2–Al_2O_3 (ref. 41) and Cu–ZnO–Al_2O_3/SAPO-11 (ref. 106) have been investigated for DME synthesis.

Wang *et al.*[1] examined the effects of CuO–ZnO–Al_2O_3/SiO_2–Al_2O_3 core–shell catalysts and physically mixed hybrid catalysts on CO conversion and DME selectivity in a fixed-bed reactor at 5.0 MPa, 260 °C, and 1500 mL h^{-1} g_{cat}^{-1}. The core–shell catalyst exhibited CO conversion and DME selectivity of 28.3% and 51.6%, respectively, whereas the physically mixed catalyst demonstrated CO conversion and DME selectivity of 71.1% and 61.9%, respectively.[31] Phienluphon *et al.* compared the activity of Cu–ZnO–Al_2O_3/SAPO-11 catalysts prepared *via* physical coating (core–shell structure) and various mixing methods in a fixed-bed reactor at 250 °C and 5.0 MPa.[106] The syngas composition was $H_2/CO/CO_2/Ar$ = 58.10 : 33.80 : 5.10 : 3.09. The core–shell Cu–ZnO–Al_2O_3/SAPO-11 catalyst outperformed its counterparts in terms of CO conversion (92.0% *vs.* 64.9%), DME selectivity (90.3% *vs.* 46.6%, C-based), and DME yield (83.1% *vs.* 30.2%).[106] Li *et al.*[100] developed a novel preparation method for a hybrid catalyst consisting of CuO–ZnO as the core and HZSM-5 as the shell. The high activity of this core–shell hybrid catalyst was attributed to the ordered self-assembly of the core–shell structure, which facilitated enhanced reactant diffusion and accelerated the reaction rate. Similar to the core–shell structure, a combination of HZSM-5 as the shell and Cu–ZnO–Al_2O_3 as the core was tested, demonstrating improved DME selectivity compared to conventional hybrid catalysts.[100]

The studies shows, that the synergy between the active sites for methanol synthesis and methanol dehydration significantly influences the catalytic activity and stability.[100–106] However, hybridized bifunctional catalysts may experience partial deactivation as the individual components interact with one another, leading to adverse reactions during the preparation or calcination stages.

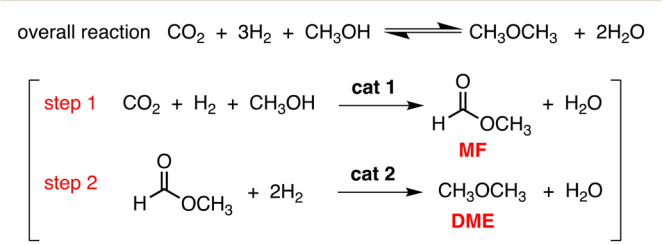

Fig. 8 Liquid-phase DME synthesis from CO_2 (DME – dimethyl ether, MF– methyl formate).

Furthermore, simultaneous processes such as Cu sintering (or aggregation), oxidation, and ion exchange on acidic sites contribute to catalyst deactivation. The efficient confinement of Cu nanoparticles within ordered mesoporous alumina and zeolite matrices has been proposed as a promising strategy for enhancing catalyst stability.

Zeolite capsule catalysts offer the advantage of increasing the selectivity of desired products by imposing strict spatial confinement on the methanol intermediate and DME.[42,106–108] Studies on CO_2 hydrogenation to DME over hybridized bifunctional catalysts have shown lower DME yields compared to the hydrogenation of CO to DME. In comparison with traditional hybrid catalysts prepared by physically mixing components, novel core–shell catalysts have garnered significant attention in the literature due to their unique structures and their enhanced ability to valorize CO_2 with improved conversion and DME selectivity.

4. Liquid phase DME synthesis – opportunities for optimization of DME productivity

4.1 New alternative two-step process of CO_2 valorization to DME in liquid phase

The liquid-phase synthesis of dimethyl ether (DME) from CO_2 using heterogeneous catalysts presents a novel and less-explored route in the field of CO_2 valorization. Our recent work demonstrates the viability of this two-step process, which offers notable thermodynamic advantages by operating under milder conditions—specifically, lower temperatures and pressures—than conventional gas-phase methods. This not only reduces energy input but also broadens the compatibility with temperature-sensitive catalytic systems. The pathway for liquid-phase CO_2 valorization *via* methyl formate is illustrated in Fig. 8. In this process, other platform chemicals, such as formic acid and methanol, which serve as intermediates, can also be investigated due to their role as important sustainable hydrogen carriers. The target product of step 1, as shown in Fig. 8, is methyl formate (MF), which then undergoes further hydrodeoxygenation in step 2 to form DME.

In step 1, the hydrogenation of CO_2 with H_2 to form formic acid in the liquid phase is entropically unfavorable. Typically, the thermodynamic equilibrium is shifted towards the product side by the addition of bases such as K_2CO_3, leading to the formation of formate salts. A range of metal complex catalysts, often incorporating ligands such as bipyridines, *N*-heterocyclic carbenes, and phosphines, has been evaluated in homogeneous systems. These catalysts typically involve non-noble metals (Fe, Ni, Cu, Co) and noble metals (Ru, Rh, Ir). Based on our findings[176] further transformation of the formate—especially in terms of neutralization—is necessary for efficient isolation of the salts in the liquid phase.

The liquid-phase process utilizes methanol both as a reagent and as a solvent. The intermediate, methyl formate (MF), could be a promising alternative to formic acid salts such as HCOOK and HCOONa. Furthermore, methanol may be generated through the hydrogenation of CO_2. The main challenge lies in the development of novel catalysts for both step 1 and step 2, particularly for the deoxygenation of MF to DME, which remains a highly demanding task.

The liquid-phase DME synthesis *via* this two-step route as a batch process can be carried out using a stainless-steel autoclave, with the process conditions controlled (maximum pressure: ~8 MPa, maximum temperature: ~180 °C, maximum stirring rate: ~1000 rpm). Our study indicates that the process efficiency below 180 °C is relatively low, with conversions typically ranging from 10–20%.[176] A significant challenge for the liquid-phase process lies in ensuring compatibility between multiple active sites, which must be carefully tailored considering factors such as reaction kinetics, mechanisms, and their interaction with reactants, products, and solvents in the same reaction environment. Therefore, major advancements in CO_2 conversion will require the development of novel catalysts and a deeper understanding of the fundamental relationships between catalyst preparation, *in situ* surface structure, and performance (Table 6).[177]

5. Process intensification strategies

5.1 Strategies for increasing DME production from CO_2-rich syngas *via in situ* H_2O removal

Direct DME synthesis from CO_2 is favored at high pressures due to the reduction in the number of moles[31] and at lower temperatures due to the exothermic nature of the target reaction. However, operation at low temperatures necessitates

Table 6 Direct gas phase *vs.* liquid-phase DME synthesis[108–177]

Aspect	Direct gas-phase DME synthesis	Liquid-phase DME synthesis (two-step process)
CO_2 conversion/yield	Higher CO_2 conversion (~20% more); greater combined DME + MeOH yield (~70% more)	Moderate conversion (~10–20%) so far; well-suited to milder conditions and catalyst tuning
Reaction conditions	High temp/pressure (210–270 °C, ~40 bar)	Lower temp/pressure (~180 °C, ~8 MPa); better workability for novel catalyst systems
Reactor complexity	Single reactor but requires complex separation units	Requires multiple stages, but avoids gas-phase dehydration, enabling simpler downstream handling
Separation/efficiency	DME purification and syngas recycle necessary; can be costly	Liquids retained in-phase; may reduce energy-intensive gas-phase separations
Catalyst design & mechanism	Bifunctional catalysts (methanol synthesis + dehydration) following surface formate pathways	Opportunities for novel ligand/support systems; control over liquid phase equilibrium and solvation

optimization of reactor designs and innovations, such as *in situ* water removal.[32] Another distinguishing factor in the direct synthesis of DME from CO_2, compared to CO, lies in the kinetics. The strongly competing reverse water–gas shift (RWGS) reaction consumes CO_2 and H_2, thus reducing selectivity towards DME. Furthermore, the water produced in the process may inhibit methanol formation, as water molecules tend to adsorb strongly on the surface of catalysts, thereby blocking the methanol formation sites.[32] Water also impacts the acid catalysts responsible for methanol dehydration, as it can degrade the structure of these catalysts. *In situ* water removal represents a potential solution to these challenges, helping to overcome thermodynamic limitations, reduce the outlet CO_2 content, and prevent catalyst deactivation due to water accumulation. Membrane separation operates effectively under steady-state conditions, whereas the use of adsorbent materials requires cyclic regeneration. The latter solution is more suitable for the process, as a low water partial pressure must be achieved within the reactor to enhance the DME synthesis process significantly. Membrane-based water removal is only effective when a constant and substantial partial pressure gradient (typically >1 bar) is maintained.[148]

Sorption-enhanced DME synthesis (SEDMES) is a novel approach for producing DME from syngas,[8,149] wherein water is removed *in situ* by a solid adsorbent. Conceptually, this is based on the principle of Le Chatelier, which asserts that reactant conversion to products in an equilibrium-limited reaction is increased by the selective removal of products. The SEDMES concept involves coupling the DME catalyst (*e.g.*, a physical mixture of methanol synthesis and dehydration catalysts or hybrid catalysts) with a solid adsorbent material that has a high capacity and selectivity for water, such as LTA zeolites (4A and 3A).[150–152] While the potential of steam sorption enhancement has been proven theoretically and experimentally for other water-releasing processes, such as the RWGS reaction,[153] methanation,[154,155] and methanol synthesis[156,157] the literature on SEDMES remains limited. The first experimental investigation into liquid-phase SEDMES was conducted by Kim *et al.*[158] In the past three years, attention has grown regarding SEDMES in gas-phase processes, as this could potentially enhance DME productivity from CO_2-rich syngas. Some studies on the direct synthesis of DME are available in the literature.[115,159–165] Although theoretical models on SEDMES[87,88,164] and its cycling design[164] have been published, experimental studies specifically on this process remain scarce.[158,164]

Recent studies examining the effect of *in situ* water removal during DME synthesis—by incorporating sorbent materials into the reactor—have been published.[115–120,166–168] Researchers have primarily focused on the synthesis of methanol, direct DME synthesis (DDMES), and sorption-enhanced DME synthesis (SEDMES) using CO_2-rich syngas (CO_2/CO molar ratio > 1) with CZA/g-Al_2O_3 catalytic mixtures. To adjust the CO_2/CO syngas ratio, CZA catalysts were also doped with ZrO_2 and Ga_2O_3, known promoters for the RWGS reaction.

DME direct synthesis from CO_2-rich syngas using three mixtures of commercial catalysts for methanol synthesis (CZA) and condensation to DME (γ-Al_2O_3) in the gas phase at a lab scale has been shown for different catalyst mixtures.[167] The mixture with equal proportions of both catalysts yielded the highest DME productivity, while the mixture with the highest CZA/γ-Al_2O_3 mass ratio (9 : 1) exhibited the highest DME selectivity. A comparison of these results with those from other studies clearly indicates that the presence of a large CO_2 fraction in the syngas adversely affects catalytic performance, resulting in lower overall carbon conversions and DME productivity. This is due to the high productivity of H_2O in the catalytic bed, which leads to Cu particle agglomeration and a consequent decrease in CO conversion, as well as the deactivation of the γ-Al_2O_3 catalyst, which reduces methanol conversion to DME. The removal of water by an adsorbent material, such as zeolite 3A, within the catalytic bed resulted in higher DME productivity. However, this effect was transient, and once the zeolite became saturated, both carbon conversion and DME productivity decreased.

An apparent positive effect on DME productivity due to *in situ* water removal can be observed at times on stream (TOS) <5 hours. DME productivity in the presence of 3A zeolite was twice as high as that obtained without zeolite (Fig. 9).[33] Furthermore, the CO_2 conversion (16%) and DME/methanol ratio (10.4) at the reactor outlet exceeded the equilibrium values of 13% and 2.6, respectively. This observation supports the notion that SEDMES is a promising approach to enhance DME production from CO_2-rich syngas. However, it should be noted that the enhancement in productivity (and selectivity) for DME declines with time on stream. After 5 hours, DME productivity returned to levels similar to those observed without zeolite, likely due to the saturation of the 3A zeolite.

van Kampen *et al.*[164,165] conducted an extended proof of concept for the gas-phase SEDMES process, examining the

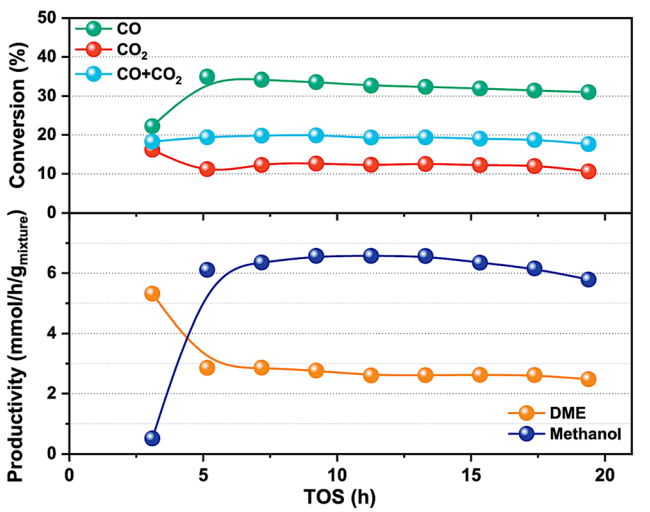

Fig. 9 Evolution of conversions and productivities obtained with the mixture 50 : 50 CZA : γ-Al_2O_3 combined with the zeolite 3A at 290 °C, 50 bar, and 5000 h^{-1}. Copyright[33] 2020 Chemical Engineering Journal Advances.

influence of regeneration conditions on both catalyst and adsorbent performance. Thermodynamic modeling was performed using Aspen Plus®, and transient experiments were carried out for various feed compositions, including inert gases such as N_2 and Ar. The study utilized a commercial $Cu/ZnO/Al_2O_3$ catalyst and a commercial zeolite A as the steam adsorbent. Adsorption experiments were performed at 275 °C and 25 bar(a), with different feed gas compositions. Regeneration of the system was achieved by switching to dry gas, followed by depressurization and heating to temperatures between 300–400 °C.[149]

The flexibility of the feed composition is achieved, as the sorption enhancement is consistent across varying CO/CO_2 ratios in the feed, as shown in Fig. 10a. In the direct synthesis of DME, 4–50% of the feed carbon is converted to DME. However, with the implementation of the SEDMES process, this conversion is significantly improved, reaching 65% or higher. Concurrently, the amount of carbon converted to CO_2 is drastically reduced, with only 2% or less being directed to CO_2, which simplifies the subsequent separation and recycling processes. These findings demonstrate the considerable strengths of the SEDMES approach in enhancing DME production. Fig. 10b illustrates the experimentally observed increase in DME conversion, highlighting that elevated regeneration temperatures contribute to higher conversion rates, ultimately leading to nearly pure DME alongside unreacted CO. Collectively, the findings presented in recent studies emphasize the beneficial impact of *in situ* water removal for DME direct synthesis from CO_2-rich syngas, thereby paving the way for sustained water removal in this process.[115–120,161–166]

5.2 Reactive distillation (RD) of MeOH to DME – an alternative to simplify DME production.

When discussing the cost-effective production of green DME, it is essential to consider the role of the reactive distillation (RD) process. The RD approach integrates both reaction and distillation within a single apparatus, offering the potential to simplify the continuous DME production process without the need for expensive or sensitive materials and components. Moreover, liquid-phase synthesis allows for the application of reactive distillation, which, on the one hand, has the potential to significantly reduce plant complexity and investment costs and, on the other hand, enables the feeding of crude methanol (MeOH) during the reaction, with simultaneous *in situ* water removal.

The dehydration of MeOH to DME is particularly suited for reactive distillation due to three key reasons: (a) the reaction is limited by chemical equilibrium, (b) the reaction is exothermic, enabling the utilization of the reaction enthalpy to reduce the heat demand for the reboiler, and (c) the components MeOH, DME, and water exhibit significant differences in their relative volatilities, facilitating effective separation.[169]

In the RD approach illustrated in Fig. 11a, crude MeOH in liquid form is introduced at the top of the reactive section of the RD column, where it flows downward. Unlike conventional DME synthesis, MeOH is dehydrated in the liquid phase, catalyzed by a solid acid catalyst fixed within a structured catalytic packing in the reaction section of the column. DME, having a higher vapor pressure than MeOH, ascends as vapor, while water, being less volatile, concentrates in the bottom section of the column. This separation process thus favors the thermodynamic formation of the product. By appropriately adjusting the design parameters of the RD system, complete conversion of MeOH can be achieved, resulting in pure DME distillate at the top and pure water at the bottom (Fig. 11b). This RD process significantly simplifies the conventional sequence of reaction, separation, and recycling.

The most innovative aspect of liquid-phase DME synthesis lies in the integration of catalytic processes with advanced reactor designs, particularly through reactive distillation (RD) and CO_2-based feedstocks. In this approach, CO_2 is hydrogenated to form methanol (MeOH) and dehydrated to DME in a continuous, one-step process. Reactive distillation is especially noteworthy as it combines the reaction and separation steps within a single apparatus, significantly simplifying the overall process. The RD process minimizes

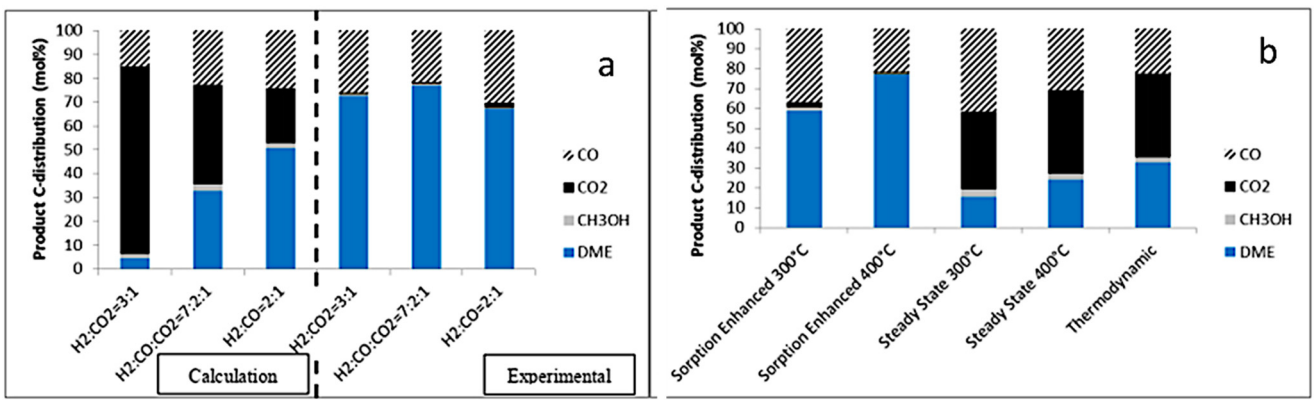

Fig. 10 a) Conventional (calculation, left) *versus* sorption enhanced (experimental, right, regeneration at 400 °C) direct DME synthesis at 25 bar(a) and 275 °C; b) carbon distribution in steady state SEDMES at 25 bar(a) and 275 °C. Copyright[149] 2020 25th International Symposium on Chemical Reaction Engineering, Florence.

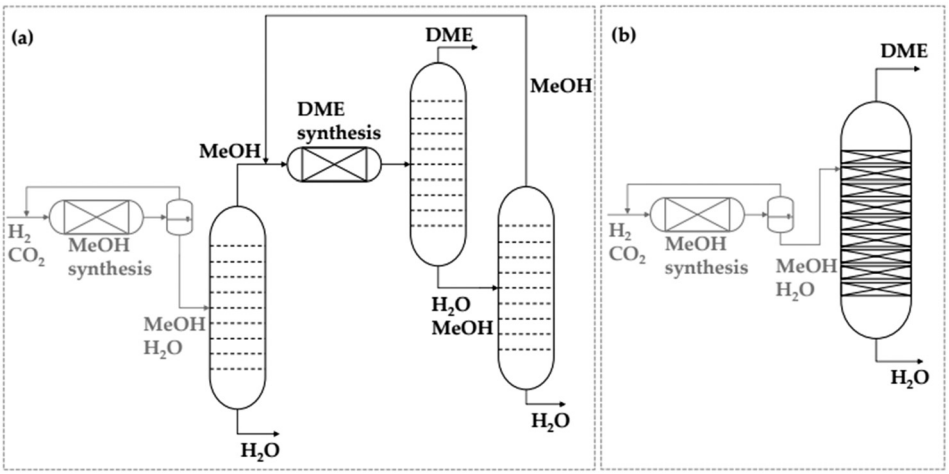

Fig. 11 Simplified flowsheet for (a) the conventional DME production process and (b) the approach by reactive distillation. Copyright[169] ChemEngineering 2022.

energy consumption, reduces equipment complexity, and allows for *in situ* water removal, which is crucial for maintaining catalyst performance. Moreover, the development of highly efficient, water-tolerant catalysts capable of operating under low-temperature (≤150 °C) and moderate-pressure (1 MPa) conditions is a key innovation. These catalysts enable better selectivity and stability, overcoming the challenges of water poisoning and reducing the need for costly separation and purification stages. This innovation paves the way for more sustainable, cost-effective DME production from renewable CO_2 resources.

The catalyst screening and reaction kinetics for liquid-phase DME synthesis under reactive distillation (RD) conditions were first presented in the literature by M. Semmel *et al.*[169–176] The study concentrates on the feasibility of implementing DME synthesis in the liquid phase under conditions typically associated with reactive distillation. The catalyst screening was conducted using a parallelized batch autoclave system. In these screening tests, two classes of cationic ion exchange resins (IER), various types of zeolites, and perfluorosulfonic acids were evaluated. Among the tested catalysts, the over-sulfonated IER A36 and the chlorinated IER CAT400 were identified as the most promising in terms of MeOH conversion and mechanical stability. The screening was conducted at temperatures ranging from 150 to 170 °C.

Subsequently, Semmel *et al.*[170] validated the previously presented comprehensive economic model aimed at minimizing total production costs. These studies pioneered the demonstration of liquid-phase DME synthesis under reactive distillation conditions. Further extended the earlier work by incorporating techno-economic modeling of reactive distillation for DME production.[170] It compared gas-phase and liquid-phase DME synthesis routes, demonstrating that liquid-phase processes could reduce costs by 27–39%. Semmel's work introduced the concept of using solid acid catalysts in liquid-phase methanol dehydration within reactive distillation, significantly reducing energy consumption and process complexity for DME production. The conventional gas-phase DME production process (used as a benchmark) and the liquid RD process using both pure MeOH feed and water-rich (crude) MeOH feed were simulated and assessed using identical technical and economic parameters. The advantages of the RD liquid process, particularly when coupled with a high-temperature stable IER catalyst, led to significant cost reductions across all considered process concepts. The higher reaction rate, enabled by the increased operating temperature of this catalyst, was a key factor in these reductions. In the integrated process concept using H_2 and CO_2 as sustainable feedstocks, the reactive distillation process resulted in a 27% reduction in production costs when crude methanol was directly fed into the DME process, bypassing the need for a dedicated methanol purification column. Further techno-economic optimization could be achieved by supplementing the RD column with an additional reactor. Ultimately, the combined RD column and side reactor concept emerged as the most promising process design, yielding a 39% reduction in production costs compared to the conventional gas-phase process. Thermal integration with a CO_2-based MeOH plant further enhances the DME production technology, eliminating the need for external heat and achieving a net conversion cost of €54.4 per tonne of DME.

6. Summary and future perspectives

Biofuel consumption in transportation will need to nearly triple by 2030, hitting 298 Mt oil equivalent, which would account for 9% of global transportation fuel demand, up from the current level of about 3%.[175] The direct conversion of CO_2 to DME presents a compelling route for sustainable fuel synthesis within a circular carbon economy. Achieving this at scale could significantly reduce GHG emissions, while offering a viable alternative to fossil-derived fuels. However, despite recent advances in catalysis and reactor engineering,

Table 7 Key economic obstacles and bottlenecks for direct CO_2-to-DME

Issue	Description	Environmental impact	Ref
High catalyst costs and development	The development of highly active and stable catalysts for the direct CO_2 hydrogenation process is still in the early stages. Catalysts for CO_2 hydrogenation to methanol and methanol dehydration to DME require bifunctionality (redox and acid functions), which adds to their complexity and cost. The use of noble metals (such as Ru, Rh, and Pd) or other advanced materials increases catalyst costs. Additionally, catalyst deactivation due to water poisoning or coke formation further complicates long-term economic viability, requiring more frequent catalyst regeneration or replacement, adding to operational costs	*Catalyst life cycle and deactivation* Catalysts used in DME production (especially bifunctional and core–shell catalysts) can experience deactivation over time due to factors like sintering, coke formation, or poisoning, which would necessitate periodic replacement or regeneration. The lifecycle impact of catalysts (including production, use, and disposal) must be considered, as these processes might contribute to the environmental burden, especially if the catalyst components are scarce or toxic	171, 176
Energy consumption	Energy costs are a significant factor in the overall economics of the CO_2-to-DME process. While the process is potentially more energy-efficient than traditional gas-phase methods, achieving low-temperature liquid--phase synthesis still requires substantial energy inputs, especially in terms of H_2 production and maintaining the required reactor conditions. If the H_2 needed for CO_2 hydrogenation is derived from fossil fuels rather than renewable sources, the overall carbon footprint of the process will increase, thus undermining the economic advantage of the CO_2-based DME production process. Additionally, processes like reactive distillation that combine reaction and separation may reduce energy demand, but they still require optimized heat integration and advanced separation techniques to lower overall energy consumption	*Energy efficiency* Energy demand: the CO_2 hydrogenation process itself requires significant energy, particularly at the high temperatures and pressures necessary for effective catalytic conversion. The energy efficiency of the process depends on the type of catalyst used and the overall process design. High-energy processes could potentially increase the carbon footprint unless low-carbon or renewable energy sources are employed	171, 176, 177
Hydrogen supply and cost	The H_2 required for CO_2 hydrogenation is another critical economic factor. If renewable H_2 (produced *via* water electrolysis) is used, its cost can be high, especially without subsidies or large-scale production. Even though H_2 production from renewable sources is expected to decrease in price over time, it remains a substantial cost barrier. H_2 storage, transportation, and integration into the process also add to the cost, especially when considering large-scale operations	*Hydrogen source* DME production from CO_2 typically requires the use of H_2 (*via* CO_2 hydrogenation). The energy used to produce H_2 plays a key role in the overall environmental impact H_2 production: the H_2 required for the reaction can be produced *via* different methods, with the most common being natural gas reforming or electrolysis using renewable energy. If fossil fuels are used for H_2 production (*e.g.*, *via* natural gas reforming), it can offset the benefits of CO_2 utilization by generating additional CO_2 emissions. However, if renewable energy sources like wind or solar power are used for electrolysis (green H_2), the process can be close to carbon neutral	171, 178, 179
CO_2 source and capture	Sourcing CO_2 for conversion into DME is another key consideration. Direct air capture (DAC) of CO_2 or capturing CO_2 from industrial processes (such as cement or steel production) can be expensive. The CO_2 capture technologies cost, although decreasing with technological advancements, remains a bottleneck for widespread adoption. The cost-effectiveness of the CO_2 feedstock must be factored into the overall economic equation, particularly if CO_2 is captured from more diffuse sources, which is less economical compared to capturing CO_2 from concentrated sources	*CO_2 recycling and carbon footprint reduction* One of the main environmental benefits of producing DME from CO_2 is that it is a form of carbon recycling. CO_2 utilization (one of GHG) as a feedstock, this process helps reduce the amount of CO_2 released into the atmosphere. The captured CO_2, ideally from industrial emissions or directly from the air (direct air capture, DAC), is converted into a useful chemical (DME), thus contributing to carbon sequestration. This approach can be considered part of the broader carbon capture and utilization (CCU) strategy, which aims to mitigate climate change by reducing atmospheric CO_2 levels	178–183
Scalability and infrastructure	The industrial-scale adoption of CO_2-to-DME processes requires significant investment in infrastructure, such as reactors, separation units, and downstream processing. The need for highly integrated systems (*i.e.* integrating CO_2 hydrogenation and methanol dehydration in a single unit) adds complexity, requiring precise engineering and optimization to ensure reliability and cost-efficiency. Developing the infrastructure for large-scale, continuous operation will require substantial capital investment, especially when considering the development and construction of plants that integrate both CO_2 capture and DME synthesis	*Potential for sustainable DME production* In terms of sustainability, DME production from CO_2 has great potential Circular economy: if CO_2 is captured from renewable sources (*e.g.*, bioenergy with carbon capture and storage, BECCS), and H_2 is produced *via* renewable energy, the entire process could be part of a circular carbon economy, contributing to long-term sustainability Energy storage: DME could also serve as an energy carrier and storage medium, helping to offset not constant renewable energy supplies (wind and solar)	172, 181–184

Table 7 *(continued)*

Issue	Description	Environmental impact	Ref
Market competition and product pricing	DME is not yet a widely used fuel compared to other alternatives such as biofuels or H_2. Therefore, the DME price must be competitive with existing fuels, including natural gas and methanol, which are produced from lower-cost processes, such as steam reforming of natural gas. Additionally, since DME production from CO_2 requires high energy inputs, ensuring that the final product is economically viable on the market remains a significant challenge. There is also competition from biomass-based DME production, which might be more cost-effective in certain regions	*DME as a clean fuel* DME is considered an environmentally friendly fuel due to its clean combustion characteristics *Low particulate emissions*: DME burns almost cleanly with negligible soot and particulate emissions, which is advantageous in reducing air pollution in urban environments *Low NO_x emissions*: the combustion of DME generates fewer nitrogen oxides (NO_x), contributing to lower smog formation and air quality improvement *No sulfur content*: DME has no sulfur content, which means it does not contribute to acid rain or sulfur-related air pollution. Thus, DME is often promoted as an alternative to conventional diesel in transportation and as a clean fuel for heating and power generation	175, 180–187
Capital and operational costs	Establishing facilities for the CO_2-to-DME conversion process, especially with reactive distillation or other advanced systems, involves high initial capital expenditure. Operating and maintaining these systems requires specialized equipment and skilled labor. The complexity of the process, with integrated catalytic and separation steps, means that operational costs might be higher compared to conventional DME production methods. Although reactive distillation can simplify the process, it requires careful design to reduce capital and operational costs	*Water usage* Water is another important consideration. While DME production does not require as much water as biofuels or other processes, water use can still be significant in terms of cooling, chemical reactions, and H_2 production. This may be more relevant if the process uses large-scale H_2 production or if water is sourced from regions with scarce water resources	175, 180–187
Regulatory and policy factors	The development and adoption of CO_2-based DME production will also depend on government policies and incentives aimed at reducing GHG emissions. Without supportive policies, such as carbon taxes, renewable energy incentives, or subsidies for carbon capture and utilization technologies, the economic viability of CO_2-to-DME processes could be limited. Regulatory frameworks that encourage low-carbon technologies will play a key role in the long-term feasibility of DME production from CO_2	Economic feasibility and scale-up While CO_2-to-DME process shows promise environmentally, the economic feasibility of large-scale DME production remains a challenge. High energy demand and the cost of H_2 production, especially from renewable sources, need to be addressed to make CO_2-based DME production competitive with traditional fuels and chemical feedstocks. Scaling up the technology while maintaining efficiency and low environmental impact will be crucial	175, 180–187

industrial implementation remains constrained by several interrelated technical and economic barriers.

Recent advancements in CO_2-to-DME technology have centered around four main areas.

• Catalyst development

Bifunctional catalysts capable of catalysing both CO_2 hydrogenation to methanol and methanol dehydration to DME have shown promise. Metal-based systems (*e.g.*, Cu/ZnO, In_2O_3–ZrO_2) for CO_2 activation paired with solid acids (*e.g.*, γ-Al_2O_3, ZSM-5, SAPO-34) for dehydration are widely studied. Recent efforts focus on spatially controlled architectures, such as core–shell and dual-bed configurations, to prevent competitive site interference and water-induced deactivation.

• Catalyst stability under harsh conditions

Water formed during both CO_2 hydrogenation and methanol dehydration is a major deactivating agent. Water-tolerant acidic supports and hydrophobic coatings (*e.g.*, organosilane-functionalized zeolites) have demonstrated improved resistance. However, long-term operation under high water partial pressures (>0.5 atm), elevated temperatures (220–280 °C), and pressures (3–8 MPa) remains a key challenge. Quantitative metrics for performance include:

CO_2 conversion >30%,

DME selectivity >90%,

Catalyst lifetime >1000 hours with <10% activity loss.

• Process intensification and reactor design

Innovations such as reactive distillation (RD) and liquid-phase synthesis enhance equilibrium-limited reactions by enabling *in situ* product separation. RD systems utilizing structured packings or zeolite-coated internals enable simultaneous reaction and water removal. Liquid-phase processes using solvents like polyols or ionic liquids show promise for

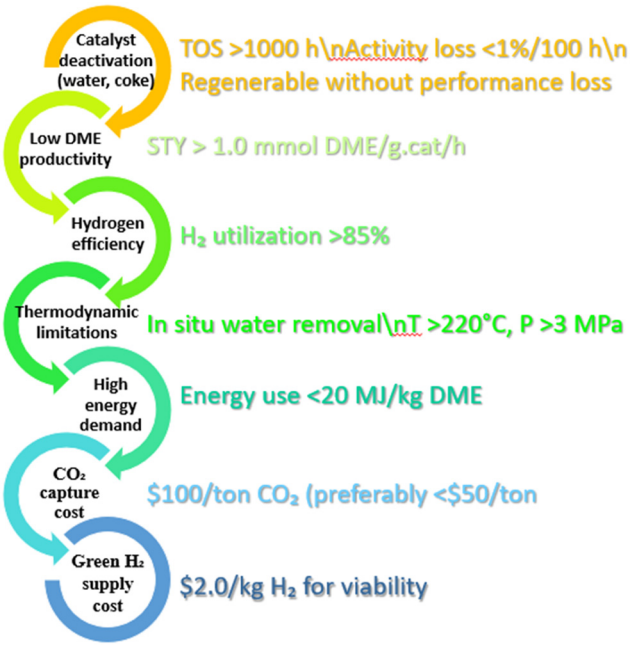

Fig. 12 Key technical and economic bottlenecks, along with benchmark performance targets needed for industrial viability direct CO_2-to-DME.

operation below 150 °C, but face kinetic limitations due to mass transfer and low solubility of CO_2 and H_2.

• Integration of CO_2 hydrogenation and methanol dehydration

One-pot systems are attractive for reducing capital costs and simplifying process flow. However, achieving optimal contact between redox and acid sites, without promoting side reactions (*e.g.*, CO formation, olefin production), requires fine control over catalyst architecture and reaction conditions.

Despite these promising developments, several technical and economic barriers remain. Table 7 highlights key bottlenecks, including high catalyst costs, energy intensity, hydrogen sourcing, and limited infrastructure. Particularly, the availability and affordability of green hydrogen and scalable CO_2 capture technologies will largely determine the feasibility of CO_2-to-DME systems.

The key challenges and performance metrics that have to be addressed to reach industrial relevance are summarized in Fig. 12.

The liquid-phase DME synthesis approach, though attractive for its lower energy consumption and compatibility with intermittent renewable energy, requires catalysts active at mild conditions (<150 °C, ~1 MPa). Most conventional catalysts underperform under these parameters, making low-temperature catalyst innovation an urgent priority. Furthermore, understanding the structure–activity relationships and the impact of water on active sites will be crucial for performance optimization.

However, to achieve industrial scalability and climate impact, future research must pursue several directions, among others:

- Catalyst design for H_2O-tolerance and low-temperature activity, *i.e.* (i) materials with engineered surface hydrophobicity, (ii) metal–support interactions development and intermediates stabilization under high H_2O partial pressures, or (iii) non-traditional catalytic systems exploration, *e.g.*, metal–organic frameworks (MOFs), heteropoly acids, or dual-phase systems. The future of direct CO_2-to-DME synthesis will depend on the convergence of catalytic innovation, process engineering, and renewable energy integration. Emerging catalyst systems—such as hybrid or core–shell structures—promise improved functionality and selectivity. Reactor designs incorporating membrane separation or advanced heat integration can further enhance efficiency.
- Advanced reactor configurations *i.e.* (i) scaling-up the reactive distillation columns with integrated heat management, (ii) membrane reactors development for selective water and methanol removal, or (iii) alternative reactors development to thermocatalytic processes *e.g.* electrochemical or plasma-assisted.
- Integration with renewable energy and CO_2 capture *i.e.* (i) couple the process with electrolyzers powered by solar/wind, ensuring intermittent compatibility *via* thermal storage or hybrid schemes, (ii) modular CO_2-to-DME units development co-located with emission sources (cement, steel), utilizing point-source or direct air capture (DAC) CO_2. Direct CO_2-to-DME synthesis to be economically and environmentally viable, it must be coupled with renewable H_2 production and low-cost CO_2 capture, ideally from industrial point sources or DAC. In this context, DME serves not only as a low-emission fuel but also as a carbon-neutral energy carrier, potentially contributing to energy storage and circular carbon strategies.
- Digital tools and modelling *i.e.* (i) machine learning employment and multiscale modeling to accelerate catalyst discovery, (ii) process simulation (*e.g.*, Aspen Plus, gPROMS) for lifecycle assessment (LCA) and techno-economic analysis (TEA), (iii) predictive structure–performance relationships for catalyst optimization. Digital tools such as process simulation, data-driven optimization, and machine learning will play an increasingly important role in accelerating research and scaling up. These technologies can help bridge the gap between lab-scale success and commercial application, supporting the broader deployment of CO_2-based fuels in a low-carbon economy.

As summarized above the transition from lab-scale demonstrations to industrial deployment, a multi-pronged strategy is required—encompassing catalyst innovation, system integration, and policy support. If coupled with renewable H_2 and cost-effective CO_2 capture, this route can enable large-scale carbon recycling, reduce dependency on fossil fuels, and contribute meaningfully to net-zero emissions targets.

Conflicts of interest

The authors declare no conflicts of interest.

Data availability

No primary research results, software or code have been included and no new data were generated or analysed as part of this review.

Acknowledgements

I. S. P. acknowledges the support of the Polish Ministry of Science and Education, grant No GGPJ5/H2020/00/507550/2021.

References

1 L. Wang, X. V. Vo, M. Shahbaz and A. Ak, *J. Environ. Manage.*, 2020, **268**, 110712.
2 E. A. Quadrelli, G. Centi, J. L. Duplan and S. Perathoner, *ChemSusChem*, 2011, **4**, 1194–1215.
3 J. N. Sommar, U. A. Hvidtfeldt, C. Geels, L. M. Frohn, J. Brandt, J. H. Christensen, O. Raaschou-Nielsen and B. Forsberg, *Int. J. Environ. Res. Public Health*, 2021, **18**, 8476.
4 V. Rizos, M. Elkerbout, C. Egenhofer and J. Núñez Ferrer, *Framing the circular economy as an EU recovery opportunity*, CEPS Policy Insights No PI2020-32/ DECEMBER 2020, CEPS, 2020.
5 S. Mehra and A. K. Agarwal, in *Greener and Scalable E-fuels for Decarbonization of Transport*, 2022, ch. 10, pp. 261–291, DOI: **10.1007/978-981-16-8344-2_10**.
6 A. Bakhtyari and M. R. Rahimpour, in *Methanol*, Elsevier, 2018, pp. 281–311, DOI: **10.1016/B978-0-444-63903-5.00010-8**.
7 **https://www.eafo.eu/alternative-fuels/advanced-biofuels/BioDME**.
8 T. A. Semelsberger, R. L. Borup and H. L. Greene, *J. Power Sources*, 2006, **156**, 497–511.
9 K. Saravanan, H. Ham, N. Tsubaki and J. W. Bae, *Appl. Catal., B*, 2017, **217**, 494–522.
10 D. Kubas, M. Gierse, O. Salem and I. Krossing, *ACS Catal.*, 2023, **13**, 3960–3970.
11 M.-H. Huang, H.-M. Lee, K.-C. Liang, C.-C. Tzeng and W.-H. Chen, *Int. J. Hydrogen Energy*, 2015, **40**, 13583–13593.
12 J. W. Jeong, C.-I. Ahn, D. H. Lee, S. H. Um and J. W. Bae, *Catal. Lett.*, 2013, **143**, 666–672.
13 S. Asthana, C. Samanta, A. Bhaumik, B. Banerjee, R. K. Voolapalli and B. Saha, *J. Catal.*, 2016, **334**, 89–101.
14 J.-W. Bae, H. S. Potdar, S.-H. Kang and K.-W. Jun, *Energy Fuels*, 2008, **22**, 223–230.
15 M. Huš, V. D. B. C. Dasireddy, N. S. Štefančič and B. Likozar, *Appl. Catal., B*, 2017, **207**, 267–278.
16 N. H. Ahn, S. Seo and S. B. Hong, *Catal. Sci. Technol.*, 2016, **6**, 2725–2734.
17 O. Oyola-Rivera, M. A. Baltanás and N. Cardona-Martínez, *J. CO_2 Util.*, 2015, **9**, 8–15.
18 W.-H. Chen, C.-L. Hsu and X.-D. Wang, *Energy*, 2016, **109**, 326–340.
19 T. Nakyai, Y. Patcharavorachot, A. Arpornwichanop and D. Saebea, *Energy*, 2020, **209**, 118332.
20 K. Im-orb and A. Arpornwichanop, *Energy Convers. Manage.*, 2022, **258**, 115511.
21 G. A. Olah, A. Goeppert and G. K. S. Prakash, *J. Org. Chem.*, 2009, **74**, 487–498.
22 C. Peinado, D. Liuzzi, S. N. Sluijter, G. Skorikova, J. Boon, S. Guffanti, G. Groppi and S. Rojas, *Chem. Eng. J.*, 2024, **479**, 147494.
23 A. Giuliano, E. Catizzone and C. Freda, *Int. J. Environ. Res. Public Health*, 2021, **18**, 807–807.
24 C. Jia, J. Gao, Y. Dai, J. Zhang and Y. Yang, *J. Energy Chem.*, 2016, **25**, 1027–1037.
25 Z. Qin, T. Su, H. Ji, Y. Jiang, R. Liu and J. Chen, *AIChE J.*, 2015, **61**, 1613–1627.
26 J. Ereña, I. Sierra, A. T. Aguayo, A. Ateka, M. Olazar and J. Bilbao, *Chem. Eng. J.*, 2011, **174**, 660–667.
27 Z. Qin, X. Zhou, T. Su, Y. Jiang and H. Ji, *Catal. Commun.*, 2016, **75**, 78–82.
28 A. Hankin and N. Shah, *Sustainable Energy Fuels*, 2017, **1**, 1541–1556.
29 X. He and L. Liu, *IOP Conf. Ser.: Earth Environ. Sci.*, 2017, **100**, 012078.
30 X. Zhou, T. Su, Y. Jiang, Z. Qin, H. Ji and Z. Guo, *Chem. Eng. Sci.*, 2016, **153**, 10–20.
31 G. Jia, Y. Tan and Y. Han, *Ind. Eng. Chem. Res.*, 2006, **45**, 1152–1159.
32 E. Kunkes and M. Behrens, in *Chemical Energy Storage*, DE GRUYTER, 2012, pp. 413–442, DOI: **10.1515/9783110266320.413**.
33 C. Peinado, D. Liuzzi, M. Retuerto, J. Boon, M. A. Peña and S. Rojas, *Chem. Eng. J. Adv.*, 2020, **4**, 100039.
34 E. Lam, J. J. Corral-Pérez, K. Larmier, G. Noh, P. Wolf, A. Comas-Vives, A. Urakawa and C. Copéret, *Angew. Chem., Int. Ed.*, 2019, **58**, 13989–13996.
35 J. Huo, J.-P. Tessonnier and B. H. Shanks, *ACS Catal.*, 2021, **11**, 5248–5270.
36 I. Barroso-Martín, A. Infantes-Molina, F. Jafarian Fini, D. Ballesteros-Plata, E. Rodríguez-Castellón and E. Moretti, *Catalysts*, 2020, **10**, 1282.
37 H.-W. Ham, M.-H. Jeong, H.-M. Koo, C.-H. Chung and J. W. Bae, *React. Kinet., Mech. Catal.*, 2015, **116**, 173–189.
38 J. W. Jung, Y. J. Lee, S. H. Um, P. J. Yoo, D. H. Lee, K.-W. Jun and J. W. Bae, *Appl. Catal., B*, 2012, **126**, 1–8.
39 Y. Chen, S. Choi and L. T. Thompson, *ACS Catal.*, 2015, **5**, 1717–1725.
40 S. Kattel, P. Liu and J. G. Chen, *J. Am. Chem. Soc.*, 2017, **139**, 9739–9754.
41 M. Cai, V. Subramanian, V. V. Sushkevich, V. V. Ordomsky and A. Y. Khodakov, *Appl. Catal., A*, 2015, **502**, 370–379.
42 A. Bayat and T. Dogu, *Ind. Eng. Chem. Res.*, 2016, **55**, 11431–11439.
43 C. Liu, J. Kang, Z.-Q. Huang, Y.-H. Song, Y.-S. Xiao, J. Song, J.-X. He, C.-R. Chang, H.-Q. Ge, Y. Wang, Z.-T. Liu and Z.-W. Liu, *Nat. Commun.*, 2021, **12**, 2305.

44 I. S. A. Ateka, J. Ereña, J. Bilbao and A. T. Aguayo, *Fuel Process. Technol.*, 2016, **152**, 34–45.
45 A. M. Sanchez-Contador, P. Rodriguez-Vega, J. Bilbao and A. T. Aguayo, *Ind. Eng. Chem. Res.*, 2018, **57**, 1169–1178.
46 K. Singh, K. Pant and J. K. Parikh, *Fuel*, 2022, **318**, 123641.
47 J. Chen, P. Wang, X. Wang, F. Song, Y. Bai, M. Zhang, Y. Wu, H. Xie and Y. Tan, *ChemCatChem*, 2019, **11**, 1448–1457.
48 P. Ateka, M. Sanchez-Contador, J. Erena, A. Aguayo and J. Bilbao, *Int. J. Hydrogen Energy*, 2016, **41**, 18015–18026.
49 G. Arena, K. Barbera, G. Bonura, L. Spadaro and F. Frusteri, *Catal. Today*, 2009, **143**, 80–85.
50 M. Schumann, T. Lunkenbein, N. Thomas, M. Galvan, R. Schlogl and M. Behrens, *ACS Catal.*, 2015, **5**, 3260–3270.
51 Z. Li, F. Liao, X. Hong and S. C. E. Tsang, *J. Catal.*, 2016, **343**, 157–167.
52 M. Sanguineti and A. Bonivardi, *Appl. Catal., A*, 2015, **504**, 476–481.
53 P. Cai, J. Toyir and N. Homs, *Catal. Today*, 2015, **242**, 193–199.
54 D. Xiao, X. Guo and J. Yu, *Energy Technol.*, 2015, **3**, 32–39.
55 P. Fornero, D. Chiavassa, A. L. Bonivardi and M. A. Baltanas, *Catal. Today*, 2013, **213**, 163–170.
56 K. Angelo, L. Tejada, Y. Zimmermann, K. Parkhomenko and A. C. Roger, *C. R. Chim.*, 2015, **18**, 250–260.
57 Y. Choi, D. Lee, D. Moon and K. Lee, *Mol. Catal.*, 2017, **434**, 146–153.
58 M. Melian-Cabrera and J. Fierro, *J. Catal.*, 2002, 285–294, DOI: **10.1006/jcat.2002.3677**.
59 I. Fierro and M. L. Granados, *J. Catal.*, 2002, **210**, 273–284.
60 F. Liu, M. Bai, F. Xue, X. Ma, Z. Jiang and T. Fang, *Mol. Catal.*, 2019, **466**, 26–36.
61 H. Pasupulety, Y. Alhamed, A. Alzahrani, M. Daous and L. Petrov, *Appl. Catal., A*, 2015, **504**, 308–318.
62 H. Pasupulety, Y. Alhamed, A. Alzahrani, M. Daous and L. Petrov, *C. R. Acad. Bulg. Sci.*, 2015, **68**, 1511–1518.
63 C. Martin, D. Curulla-Ferre, C. Drouilly, R. Hauert and J. Perez-Ramírez, *ACS Catal.*, 2015, **5**, 5607–5616.
64 C. Wang, T. Senftle, J. Zhu, G. Zhang, X. Guo and C. Song, *ACS Catal.*, 2020, **10**, 3264–3273.
65 G. Wang, J. Zhu, X. Zhang, F. Ding, A. Zhang, X. Guo and C. Song, *ACS Catal.*, 2021, **11**, 1406–1423.
66 C. Ye, D. Mei and Q. Ge, *ACS Catal.*, 2013, **3**, 1296–1306.
67 C. Frei, A. Cesarini, F. Krumeich, R. Hauert, J. A. Stewart, D. C. Ferre and J. Perez-Ramírez, *ACS Catal.*, 2019, **10**, 1133–1145.
68 M. Frei, R. García-Muelas, C. Mondelli, N. Lopez, J. Stewart, D. Curulla-Ferré and J. Perez-Ramírez, *J. Catal.*, 2018, **361**, 313–321.
69 A. Martin, C. Mondelli, S. Mitchell, T. Segawa, R. Hauert, C. Drouilly, D. Curulla-Ferré and J. Perez-Ramírez, *Angew. Chem., Int. Ed.*, 2016, **55**, 6261–6265.
70 C. Chen, T. Chen, X. Ding, H. Huang, L. Shen, X. Cao, M. Zhu, J. Xu, J. Gao and Y. Han, *ACS Catal.*, 2019, **9**, 8785–8797.
71 G. Wang, Z. Li, C. Tang, Z. Feng, H. An, H. Liu, T. Liu and C. Li, *Sci. Adv.*, 2017, **3**, e1701290.
72 G. Li, W. T. Ralston, K. An, C. Brooks, Y. Ye, Y. Liu, J. Zhu, J. Guo, S. Alayoglu and G. Somorjai, *Nat. Commun.*, 2015, **6**, 1–5.
73 D. Stangeland, Y. Ding and Z. Yu, *J. CO2 Util.*, 2019, **32**, 146–154.
74 E. Wang, Y. Wang, L. Wang, Z. Gong, Y. Cui, X. Meng, B. Gates and F. Xiao, *Nat. Commun.*, 2020, **11**, 1–9.
75 S. Malik, A. Al-Zahrani and M. Daous, *J. Ind. Eng. Chem.*, 2021, **103**, 67–79.
76 M. Bahruji, G. Hutchings, N. Dimitratos, P. Wells, E. Gibson, W. Jones, C. Brookes, D. Morgan and G. Lalev, *J. Catal.*, 2016, **343**, 133–146.
77 M. Bahruji, W. Jones, J. Hayward, J. R. Esquius, D. J. Morgan and G. J. Hutchings, *Faraday Discuss.*, 2017, **197**, 309–324.
78 D. Hartadi and R. J. Behm, *ChemSusChem*, 2015, **8**, 456–465.
79 D. Hartadi and R. J. Behm, *J. Catal.*, 2016, **333**, 238–250.
80 D. Hartadi and R. J. Behm, *Phys. Chem. Chem. Phys.*, 2016, **18**, 10781–10791.
81 P. Wu, Z. Zhang, L. Zhang, G. Yang and B. Han, *ChemCatChem*, 2017, **9**, 3691–3696.
82 H. Ham, J. Kim, S. J. Cho, J.-H. Choi, D. J. Moon and J. W. Bae, *ACS Catal.*, 2016, **6**, 5629–5640.
83 A. Aloise, F. Dalena, G. Giorgianni, M. Migliori, L. Frusteri, C. Cannilla, G. Bonura, F. Frusteri and G. Giordano, *Microporous Mesoporous Mater.*, 2020, **302**, 110198.
84 Y. Zeng, J. Mou, F. Liu, C. Yang, T. Zhao, X. Wang and J. Cao, *Int. J. Hydrogen Energy*, 2020, **45**, 16500–16508.
85 M. Hosseini and F. Yaripour, *J. Energy Chem.*, 2011, **20**, 128–134.
86 X. Chen, Y. Xu, Y. Dong, W. Lai, W. Fang and X. Yi, *Catal. Commun.*, 2018, **103**, 1–4.
87 A. Seker, V. Balci and A. Uzun, *Renewable Energy*, 2021, **171**, 47–57.
88 A. Catizzone, M. Migliori and G. Giordano, *Appl. Catal., A*, 2015, **502**, 215–220.
89 E. Catizzone, M. Migliori, P. C. Cozzucoli and G. Giordano, *Materials*, 2020, **13**, 1–15.
90 A. Catizzone, M. Migliori and G. Giordano, *J. Energy Chem.*, 2017, **26**, 406–415.
91 M. Frusteri, C. Cannilla, L. Frusteri, E. Catizzone, A. Aloise, G. Giordano and G. Bonura, *J. CO2 Util.*, 2017, **18**, 353–361.
92 E. Catizzone, G. Bonura, M. Migliori, G. Braccio, F. Frusteri and G. Giordano, *Ann. Chim.: Sci. Mater.*, 2019, **43**, 141–149.
93 N. Mota, E. M. Ordoñez, B. Pawelec, J. L. G. Fierro and R. M. Navarro, *Catalysts*, 2021, **11**, 411–411.
94 F. Frusteri, G. Bonura, C. Cannilla, G. Drago Ferrante, A. Aloise, E. Catizzone, M. Migliori and G. Giordano, *Appl. Catal., B*, 2015, **176–177**, 522–531.
95 A. Bansode and A. Urakawa, *J. Catal.*, 2014, **309**, 66–70.
96 J. Bae, S. Kang, Y. Lee and K. Jun, *J. Ind. Eng. Chem.*, 2009, **15**, 566–572.
97 G. Yang, M. Thongkam, T. Vitidsant, Y. Yoneyama, Y. Tan and N. Tsubaki, *Catal. Today*, 2011, **171**, 229–235.
98 R. Nie, H. Lei, S. Pan, L. Wang, J. Fei and Z. Hou, *Fuel*, 2012, **96**, 419–425.

99 W. Jiyuan and Z. Chongyu, *J. Nat. Gas Chem.*, 2005, **14**, 156–162.
100 Q. Li, C. Xin and P. Lian, *Pet. Sci. Technol.*, 2012, **30**, 2187–2195.
101 S. M. Solyman, N. A. K. Aboul-Gheit, M. Sadek, F. M. Tawfik and H. A. Ahmed, *Egypt. J. Pet.*, 2015, **24**, 289–297.
102 H. Jung, F. Zafar, X. Wang, T. X. Nguyen, C. H. Hong, Y. G. Hur, J. W. Choung, M. Park and J. Bae, *ACS Catal.*, 2021, **11**, 14210–14223.
103 A. Ateka, M. Sánchez-Contador, A. Portillo, J. Bilbao and A. Aguayo, *Fuel Process. Technol.*, 2020, **206**, 106434.
104 R. Liu, Z. Qin, H. Ji and T. Su, *Ind. Eng. Chem. Res.*, 2013, **52**, 16648–16655.
105 R. Liu, H. Tian, A. Yang, F. Zha, J. Ding and Y. Chang, *Appl. Surf. Sci.*, 2015, **345**, 1–9.
106 R. Phienluphon, K. Pinkaew, G. Yang, J. Li, Q. Wei, Y. Yoneyama, T. Vitidsant and N. Tsubaki, *Chem. Eng. J.*, 2015, **270**, 605–611.
107 F. Frusteri, M. Migliori, C. Cannilla, L. Frusteri, E. Catizzone, A. Aloise, G. Giordano and G. Bonura, *J. CO_2 Util.*, 2017, **18**, 353–361.
108 K. Pinkaew, G. Yang, T. Vitidsant, Y. Jin, C. Zeng, Y. Yoneyama and N. Tsubaki, *Fuel*, 2013, **111**, 727–732.
109 Y. Wang, W. Wang, Y. Chen, J. Ma and R. Li, *Chem. Eng. J.*, 2014, **250**, 248–256.
110 S. Wang, D. Mao, X. Guo, G. Wu and G. Lu, *Catal. Commun.*, 2009, **10**, 1367–1370.
111 P. Ateka, J. Ereña, A. T. Aguayo and J. Bilbao, *Fuel Process. Technol.*, 2022, **233**, 107310.
112 E. N. Mota, B. Pawelec, J. L. G. Fierro and R. M. Navarro, *Catalysts*, 2021, **11**, 411.
113 M. Bayat and A. G. Asil, *Int. J. Hydrogen Energy*, 2024, **50**, 658–673.
114 G. Bonura, M. Cordaro, L. Spadaro, C. Cannilla, F. Arena and F. Frusteri, *Appl. Catal., B*, 2013, **140–141**, 16–24.
115 N. Shimoda, H. Muroyama, T. Matsui, K. Faungnawakij, R. Kikuchi and K. Eguchi, *Appl. Catal., A*, 2011, **409–410**, 91–98.
116 L. Oar-Arteta, A. Remiro, J. Vicente, A. T. Aguayo, J. Bilbao and A. G. Gayubo, *Fuel Process. Technol.*, 2014, **126**, 145–154.
117 L. Oar-Arteta, A. Remiro, A. T. Aguayo, J. Bilbao and A. G. Gayubo, *Ind. Eng. Chem. Res.*, 2015, **54**, 9722–9732.
118 L. Oar-Arteta, A. Remiro, F. Epron, N. Bion, A. T. Aguayo, J. Bilbao and A. G. Gayubo, *Ind. Eng. Chem. Res.*, 2016, **55**, 3546–3555.
119 D. Kim, B. Choi, G. Park, K. Lee, D. Lee and S. Jung, *Chem. Eng. Sci.*, 2020, **216**, 115535.
120 J. Vicente, A. G. Gayubo, J. Ereña, A. T. Aguayo, M. Olazar and J. Bilbao, *Appl. Catal., B*, 2013, **130–131**, 73–83.
121 A. Gayubo, J. Vicente, J. Ereña, L. Oar-Arteta, M. J. Azkoiti, M. Olazar and J. Bilbao, *Appl. Catal., A*, 2014, **483**, 76–84.
122 M. Cargnello, M. Grzelczak, B. Rodríguez-González, Z. Syrgiannis, K. Bakhmutsky, V. La Parola, L. M. Liz-Marzán, R. J. Gorte, M. Prato and P. Fornasiero, *J. Am. Chem. Soc.*, 2012, **134**, 11760–11766.
123 G. Valenti, A. Boni, M. Melchionna, M. Cargnello, L. Nasi, G. Bertoni, R. J. Gorte, M. Marcaccio, S. Rapino, M. Bonchio, P. Fornasiero, M. Prato and F. Paolucci, *Nat. Commun.*, 2016, **7**, 13549.
124 M. Melchionna, A. Beltram, A. Stopin, T. Montini, R. W. Lodge, A. N. Khlobystov, D. Bonifazi, M. Prato and P. Fornasiero, *Appl. Catal., B*, 2018, **227**, 356–365.
125 A. Beltram, M. Melchionna, T. Montini, L. Nasi, P. Fornasiero and M. Prato, *Green Chem.*, 2017, **19**, 2379–2389.
126 M. Melchionna, M. V. Bracamonte, A. Giuliani, L. Nasi, T. Montini, C. Tavagnacco, M. Bonchio, P. Fornasiero and M. Prato, *Energy Environ. Sci.*, 2018, **11**, 1571–1580.
127 D. Eder, *Chem. Rev.*, 2010, **110**, 1348–1385.
128 A. Reina, R. Carmona-Chávez, I. T. Pulido-Díaz, D. Martínez, K. P. Salas-Martin and I. Guerrero-Ríos, *ChemCatChem*, 2023, **15**, e202300285.
129 A. Rodriguez-Otero, V. Vargas, A. Galarneau, J. Castillo, J. H. Christensen and B. Bouyssiere, *Processes*, 2023, **11**, 3373.
130 S. Wu, C. Mou and H. Lin, *Chem. Soc. Rev.*, 2013, **42**, 3862.
131 A. Presentato, F. Armetta, A. Spinella, D. F. Chillura Martino, R. Alduina and M. L. Saladino, *Front. Chem.*, 2020, **8**, 699, DOI: **10.3389/fchem.2020.00699**.
132 W. Li, H. Wang, X. Jiang, J. Zhu, Z. Liu, X. Guo and C. Song, *RSC Adv.*, 2018, **8**, 7651–7669.
133 K. Zhang, L. Xu, J. Jiang, N. Calin, K. Lam, S. Zhang, H. Wu, G. Wu, B. Albela, L. Bonneviot and P. Wu, *J. Am. Chem. Soc.*, 2013, **135**, 2427–2430.
134 Z. Xue, C. Lu, H. Shang, G. An, J. Zhang, S. Zhao and Y. Liu, *New J. Chem.*, 2020, **44**, 2788–2796.
135 A. García-Trenco and A. Martínez, *Catal. Today*, 2013, **215**, 152–161.
136 B. Sabour, M. H. Peyrovi, T. Hamoule and M. Rashidzadeh, *J. Ind. Eng. Chem.*, 2014, **20**, 222–227.
137 M. C. Ortega-Liebana, J. Bonet-Aleta, J. L. Hueso and J. Santamaria, *Catalysts*, 2020, **10**, 333–333.
138 O. Verho, F. Gao, E. V. Johnston, W. Wan, A. Nagendiran, H. Zheng, J.-E. Bäckvall and X. Zou, *APL Mater.*, 2014, **2**, 113316.
139 P. Hao, B. Peng, B. Shan, T. Yang and K. Zhang, *Nanoscale Adv.*, 2020, **2**, 1792–1810.
140 M. S. Khosrowshahi, A. A. Aghajari, M. Rahimi, F. Maleki, E. Ghiyabi, A. Rezanezhad, A. Bakhshi, E. Salari, H. Shayesteh and H. Mohammadi, *Mater. Today Sustain.*, 2024, **27**, 100900.
141 A. Kornas, M. Śliwa, M. Ruggiero-Mikołajczyk, K. Samson, J. Podobiński, R. Karcz, D. Duraczyńska, D. Rutkowska-Zbik and R. Grabowski, *React. Kinet., Mech. Catal.*, 2020, **130**, 179–194.
142 N. Wesner, L. Prawitt, A. Ortmann, J. Albert and M. J. Poller, *RSC Adv.*, 2025, **15**, 38–47.
143 Y. Yu, S. Wang, M. Xiao, L. Sun and Y. Meng, *Catalysts*, 2019, **9**, 320.
144 M. Ritacco, L. Caporaso, H. Detz and V. Butera, *ChemCatChem*, 2023, **15**, e202201171.
145 C. Liu, J. Kang and Z. Q. Huang, *et al.*, *Nat. Commun.*, 2021, **12**, 2305.

146 L. Yao, W. Liao, N. Rui, N. Li, Z. Liu, J. Cen, F. Zhang, X. Li, L. Song, L. B. De Leon, D. Su, S. Senanayake, P. Liu, D. Ma, J. Chen and J. Rodriguez, *ACS Catal.*, 2019, **9**, 9087–9097.
147 G. Yang, N. Tsubaki, J. Shamoto, Y. Yoneyama and Y. Zhang, *J. Am. Chem. Soc.*, 2010, **132**, 8129–8136.
148 J. van Kampen, J. Boon, F. van Berkel, J. Vente and M. van Sint Annaland, *Chem. Eng. J.*, 2019, **374**, 1286–1303.
149 J. van Kampen, J. Boon, F. van Berkel, H. A. J. van Dijk, J. F. Vente and M. van Sint Annaland, *X X I I I International Conference on Chemical Reactors*, Florence, Italy, 2018.
150 A. Gorbach, M. Stegmaier and G. Eigenberger, *Adsorption*, 2004, **10**, 29–46.
151 E. Gabruś, J. Nastaj, P. Tabero and T. Aleksandrzak, *Chem. Eng. J.*, 2015, **259**, 232–242.
152 M. Simo, S. Sivashanmugam, C. J. Brown and V. Hlavacek, *Ind. Eng. Chem. Res.*, 2009, **48**, 9247–9260.
153 B. Carvill, J. Hufton, M. Anand and S. Sircar, *AIChE J.*, 1996, **42**, 2765–2772.
154 S. Walspurger, G. Elzinga, J. Dijkstra, M. Sarić and W. G. Haije, *Chem. Eng. J.*, 2014, **242**, 379–386.
155 A. Borgschulte, N. Gallandat, B. Probst, R. Suter, E. Callini, D. Ferri, Y. Arroyo, R. Erni, H. Geerlings and A. Züttel, *Phys. Chem. Chem. Phys.*, 2013, **15**, 9620.
156 J. Terreni, M. Trottmann, T. Franken, A. Heel and A. Borgschulte, *Energy Technol.*, 2019, **7**, 1801093.
157 A. Zachopoulos and E. Heracleous, *J. CO_2 Util.*, 2017, **21**, 360–367.
158 H. Kim, H. Jung and K. Lee, *Korean J. Chem. Eng.*, 2001, **18**, 838–841.
159 Z. Azizi, M. Rezaeimanesh, T. Tohidian and M. R. Rahimpour, *Chem. Eng. Process.: Process Intesif.*, 2014, **82**, 150–172.
160 J. Sun, G. Yang, Y. Yoneyama and N. Tsubaki, *ACS Catal.*, 2014, **4**, 3346–3356.
161 A. Ateka, P. Rodriguez-Vega, J. Ereña, A. T. Aguayo and J. Bilbao, *Fuel*, 2022, **327**, 125148.
162 S. Baek, S.-H. Kang, J. W. Bae, Y. Lee, D. Lee and K. Lee, *Energy Fuels*, 2011, **25**, 2438–2443.
163 G. Celik, A. Arinan, A. Bayat, H. O. Ozbelge, T. Dogu and D. Varisli, *Top. Catal.*, 2013, **56**, 1764–1774.
164 J. van Kampen, J. Boon, J. Vente and M. van Sint Annaland, *J. CO_2 Util.*, 2020, **37**, 295–308.
165 J. L. Weber, C. Hernández Mejía, K. P. de Jong and P. E. de Jongh, *Catal. Sci. Technol.*, 2024, **14**, 4799–4842.
166 K. Faungnawakij, N. Shimoda, N. Viriya-empikul, R. Kikuchi and K. Eguchi, *Appl. Catal., B*, 2010, **97**, 21–27.
167 D. Liuzzi, C. Peinado, M. A. Peña, J. van Kampen, J. Boon and S. Rojas, *Sustainable Energy Fuels*, 2020, **4**, 5674–5681.
168 Z. Ravaghi-Ardebili and F. Manenti, *Appl. Energy*, 2015, **145**, 278–294.
169 T. Cholewa, M. Semmel, F. Mantei, R. Güttel and O. Salem, *ChemEngineering*, 2022, **6**, 13–13.
170 M. Semmel, M. Kerschbaum, B. Steinbach, J. Sauer and O. Salem, *React. Chem. Eng.*, 2023, **8**, 2826–2840.
171 In CODE Proposal nr SEP210704427, within the Horizon H2020-2018-2020 work program "Secure, clean and efficient energy" LC-SC3-RES-25-2020.
172 G. Gunasekar, K. Park, K. D. Jung and S. Yoon, *Inorg. Chem. Front.*, 2016, **3**(7), 882–895, DOI: **10.1039/c5qi00231a**.
173 M. Semmel, R. Ali, M. Ouda, A. Schaadt, J. Sauer and C. Hebling, Power-to-DME: a cornerstone towards a sustainable energy system, in *Power to Fuel*, Elsevier, 2021, pp. 123–151.
174 M. Semmel, L. Steiner, M. Bontrup, J. Sauer and O. Salem, *Chem. Eng. J.*, 2023, **455**, 140525, DOI: **10.1016/j.cej.2022.140525**.
175 International Energy Agency, *The future of biofuels: Pathways to a low-carbon transport sector*, 2020, **https://www.iea.org/reports/the-future-of-biofuels**.
176 M. Tawalbeh, R. N. Javed, A. Al-Othman and F. Almomani, *Energy Convers. Manage.*, 2023, **279**, 116755, DOI: **10.1016/j.enconman.2023.116755**.
177 R. Sun, Y. Liao, S. Bai, M. Zheng, C. Zhou, T. Zhang and B. Sels, *Energy Environ. Sci.*, 2021, **14**, 1247–1285, DOI: **10.1039/D0EE03575K**.
178 K. Lee, H. Yan, Q. Sun, Z. Zhang and N. Yan, *Acc. Mater. Res.*, 2023, **4**(9), 746–757, DOI: **10.1021/accountsmr.3c00075**.
179 D. Bulushev and J. Ross, *Catal. Rev.: Sci. Eng.*, 2018, **60**(4), 566–593, DOI: **10.1080/01614940.2018.1476806**.
180 R. Nie, Y. Tao, Y. Nie, T. Lu, J. Wang, Y. Zhang, X. Lu and C. Xu, *ACS Catal.*, 2021, **11**(3), 1071–1095, DOI: **10.1021/acscatal.0c04939**.
181 A. Lamberts-Van Assche and T. Compernolle, *Tutorial Review*, 2021, DOI: **10.21203/rs.3.rs-277248/v1**.
182 International Energy Agency, *Advanced Biofuels – Potential for Cost Reduction*, IEA Bioenergy: Task 41:2020:01, 2020, **https://task39.ieabioenergy.com**.
183 International Energy Agency, *Energy Technology Perspectives 2024*, IEA Bioenergy: Task 41:2020:01, 2024, **https://www.iea.org/reports/energy-technology-perspectives-2024**.
184 M. Anwar, A. Fayyaz, N. Sohail, M. Khokhar, M. Baqar, A. Yasar, K. Rasool, A. Nazir, M. Raja, M. Rehan, M. Aghbashlo and A. Tabatabaei, *J. Environ. Manage.*, 2020, **260**, 11005, DOI: **10.1016/j.jenvman.2019.110059**.
185 International Energy Agency, The Role of Renewable Transport Fuels in Decarbonizing Road Transport, *A Report from the Advanced Motor Fuels TCP and IEA Bioenergy TCP – Deployment-Barriers-and-Policy-Recommendations*, 2020, **https://www.ieabioenergy.com**.
186 O. Kousuke, S. Takehito, Y. Kaname, K. Yuji, I. Yuichi and S. Naoya, *Sci. Adv.*, 2023, **9**, eadf6865, DOI: **10.1126/sciadv.adf6865**.
187 M. Behrens, *Recyclable Catal.*, 2015, **2**, 78–86, DOI: **10.1515/recat-2015-0009**.